VISCOELASTIC PROPERTIES OF SILICA FIBRE REINFORCED EPOXIDES AND A THEORY OF FRACTURE OF FIBRE REINFORCED VISCO-ELASTIC MATERIALS

R. G. C. Arridge

Ministry of Defence
London, England

January 1972

UNLIMITED

BR No 28315

D Mat Report No 178

PROCUREMENT EXECUTIVE, MINISTRY OF DEFENCE

VISCOELASTIC PROPERTIES OF SILICA FIBRE REINFORCED EPOXIDES and A THEORY OF FRACTURE OF FIBRE REINFORCED VISCOELASTIC MATERIALS

by

R.G.C. Arridge

Department of Engineering Science

Oxford University

JANUARY 1972

UNLIMITED

D. Mat. Report No.178

D. Mat Ref. No.ZB/107/03

PROCUREMENT EXECUTIVE,
MINISTRY OF DEFENCE

VISCOELASTIC PROPERTIES OF SILICA FIBRE REINFORCED EPOXIDES

and

A THEORY OF FRACTURE OF FIBRE REINFORCED VISCOELASTIC MATERIALS

by

R. G. C. Arridge

Department of Engineering Science
Oxford University

January 1972

Report to Director of Research Materials 2 under former Ministry of Technology
Research Agreement No.PD/57/021

FORWORD

This report was prepared by the Department of Engineering Science, Oxford University for the Director of Research Materials 2, Procurement Executive, Ministry of Defence under former Ministry of Technology Research Agreement No.PD/57/021. The work was commenced in October, 1966. The work was planned, progressed and administered by Mat(O)1 under the direction of ADR/Mat2(O), Procurement Executive, Ministry of Defence. The work was performed by Mr. R. G. C. Arridge assisted by Mr. R. C. Stone under the supervision of Dr. N. G. McCrum.

This report covers work performed between 1966 and 1969.

SUMMARY

This report describes the measurement of shear modulus and damping of epoxy resin samples undirectionally reinforced with silica fibres. The measurements have been performed over a temperature range including the glass-rubber transition of the resin on samples cut with fibres at various angles to the specimen axis. Fibre concentrations up to 74% have been used.

The results have been compared with theoretical values derived from three different theories and fair agreement found for the glassy state of the resin. Anomalies were found in the rubber modulus and in the shape and position of the main absorption peak for the resin. The causes of these anomalies are discussed and satisfactory explanations put forward.

Section 5 of the report presents a theory of fracture of unidirectional fibre reinforced materials in which the rate at which elastic energy, released by fibre breakage, can be absorbed, is calculated.

Analogies of fibre reinforcement theory and chain fracture theories in polymers are discussed.

CONTENTS

VISCOELASTIC PROPERTIES OF SILICA FIBRE REINFORCED EPOXIDES

TV

21. Comparison of results on specimens cut with axes at 30° to fibres with theoretical calculations and control - no finish on glass fibres.
Cast 29. 31%

22. Comparison of results on specimens cut with axes at 45° to fibres with theoretical calculations and control - no finish on glass fibres.
Cast 29. 32% fibres

23. Comparison of results on specimens cut with axes at 60° to fibres with theoretical calculations and control - no finish on glass fibres.
Cast 29. 31% fibres

24. Comparison of results on specimens cut with axes at 90° to fibres with theoretical calculations and control - no finish on fibres.
Cast 29. 31% fibres

25. Comparison of results on specimens cut with axes at 0° to fibres with theoretical calculations and control - finish on fibres.
Cast 30. 41% fibres

26. Comparison of results on specimens cut with axes at 45° to fibres with theoretical calculations and control - finish on fibres.
Cast 30. 37% fibres

27. Comparison of results on specimens cut with axes at 0° to fibres with theoretical calculations and control - no finish on fibres.
Cast 33. 74% fibres

28. Comparison of results on specimens cut with axes at 0° to fibres with theoretical calculations and control - no finish on fibres.
Cast 42. 58% fibres

29. Comparison of results on specimens cut with axes at 0° to fibres with theoretical calculations and control - finish on fibres.
Cast 34. 48% fibres

30. Comparison of results on specimens cut with axes at 0° to fibres with theoretical calculations and control - no finish on fibres.
Cast 43. 54% fibres

31. Graph of predicted failing strain against fibre concentration for $r_f = 100\mu$, $\bar{\epsilon} = 0{\cdot}01$

32. Graph of predicted failing strain against fibre concentration for $r_f = 10\mu$, $\bar{\epsilon} = 0{\cdot}01$

33. Graph of predicted failing strain against fibre concentration for $r_f = 100\mu$ $\bar{\epsilon} = 0{\cdot}1$

34. Graph of predicted failing strain against fibre concentration for $r_f = 10\mu$, $\bar{\epsilon} = 0{\cdot}1$

LIST OF SYMBOLS USED

T_g	Glass transition temperature
tan δ	Damping factor
G	Shear modulus N/m^2
α peak	The tan δ peak at the T_g
C_{11} C_{12} etc.	Elastic stiffnesses in tensor form
S_{11} S_{12} etc.	Elastic compliances in tensor form
E	Young's modulus
E_1	Young's modulus along 1 - axis
E_2	Young's modulus along 2 - axis
ν_{11} ν_{12} etc.	Poisson's ratios as defined
S^1_{55}	Elastic compliance in transformed axes
G0, G30 etc.	Shear modulus of specimens cut with axes at 0^0, 30^0 etc. to the fibres
S_{ij}	Tensor of complex compliances
G_F	Shear modulus of the fibres N/m^2
G_M	Shear modulus of the resin N/m^2
λ	A constant
I	Moment of inertia about the axis of rotation
θ	Angle of rotation
$\ddot{\theta}$	Angular acceleration of torsional system
$\dot{\theta}$	Angular velocity of torsional system
t	time
κ, k, κ'	Constants in equation for torsional oscillations
G_o	Characteristic surface energy
P_c	Applied load at instant of fast crack extension
b	Specimen thickness
C	Specimen compliance
a	Crack length

τ	Shear stress
E_f	Young's modulus of the fibre
G_m	Shear modulus of the resin
ϵ	Overall strain in the composite
$2R$	Mean separation of fibres laterally
r_f	Fibre radius
$l/2$	Elastic transfer length
β	As defined in paper
σ	Tensile stress
E_c	Elastic strain energy in the zone before fibre fracture
σ_c	Tensile stress in composite
E_{bf}	The strain energy in the two broken fibres
E_m	The energy in the matrix material
γ_f	Surface energy of fibre
γ_m	Surface energy of resin
F	Cumulative distribution function
f	Probability function
σ	Standard deviation
$\bar{\epsilon}$	Mean strain
N_0	Number of fibres in bundle
T	Retardation time
N	Number of fibres at time t
E_u	Unrelaxed Young's modulus
E_R	Relaxed Young's modulus

1. INTRODUCTION

The improvement of the properties of synthetic resins, of both the thermosetting and the thermoplastic types, by the incorporation of high strength, high modulus fibres is by now a well-known technique. A great deal of practical knowledge on glass reinforced polyester and epoxide resins has been obtained and some theoretical studies of the elastic moduli and the fracture mechanics of such assemblies have also been made. (see e.g. Broutman-Krock (20)).

The number of variations possible in a fibre reinforced material allows the engineer to consider designs in which the most efficient use of material can be planned for any particular component. However before any exact theory can be established the properties of the "unit cell" - the fibre-matrix unit must be determined and understood in terms of the mechanical properties of each component.

In the general case neither the fibre nor the matrix material is an elastic solid in the Hookean sense. The fibre usually approximates better to this ideal than does the matrix although carbon fibres show a marked anisotropy of elastic moduli and some other types of fibre show viscoelastic properties. A resin matrix is, to a first approximation, linearly viscoelastic while a metal one possesses a yield point and the characteristics of a crystalline material with defects.

Several theories have now been put forward for predicting the elastic behaviour of a fibre composite from its constituents. Hashin and Rosen, (1) and Hill, (2) give upper and lower bounds on the elastic moduli which are rigorous for the models used. Whitney and Riley (3) solve the problem of the composite cylinder and use this model to predict properties of an assemblage of such cylinders. Savin and Van Fo Fy (4) solve the equations of equilibrium for a hexagonal array of fibres in a matrix under applied stress using an elliptic function expansion and integrate to find the composite elastic moduli. A numerical solution of the stress equations for a square array has also been produced by Heaton (5) and integrated to yield the elastic moduli. Similar calculations have also been made by Pickett (6) and Chen and Cheng.(7) A very full review of the theories is given by Chamis and Sendeckyj.(8)

There has been little experimental confirmation of any of the theories except for the case of longitudinally applied stresses. The results of Whitney and Riley for example for shear stress indicate that a large discrepancy may exist between predicted values and those actually measured.

In a specimen reinforced with fibres all parallel to its longitudinal axis the longitudinal Young's modulus is greatly affected by reinforcement. Seventy percent glass reinforcement increases the modulus 14 times and a similar proportion of carbon or boron fibres increases it 70 times. Yet the transverse Young's modulus and the longitudinal shear modulus are only increased at the most by a factor of 4 or 5 over those of the pure resin. Consequently the composite elastic properties most affected by the properties of the resin are the transverse Young's modulus and the shear moduli.

There appear to be no published results on fibre reinforced viscoelastic materials which can be related to theory when the time dependent quantities are substituted in the theoretical equations.

The work reported was therefore undertaken in an attempt to discover whether the relations derived by Hashin, Hill, Savin and Van Fo Fy and others were applicable to fibre reinforced systems with time dependent mechanical properties.

2. PROGRAMME

In order to obtain a high modulus in the fibre direction, commercially produced fibre-resin composites incorporate as many fibres as possible. Consequently, fibres are packed in bundles and the array cured under pressure in order to eliminate voids and expel excess resin. The resulting material usually has an irregular distribution of fibres and in the fibre direction, numerous cross-overs must occur. Although auch a material can be considered as approximating to a hexagonal close packed array, it is likely that important physical differences may exist because of the irregularity of the packing. Furthermore, the properties of the fibres and resin used in the composites are not disclosed. The object of this research was to make a study of fibre concentration and its effect on elastic properties. It was therefore necessary to experiment with composites with accurately spaced fibres in a regular array. The use of thick rods which could easily be arranged in any desired array, was ruled out on the grounds that to achieve a macroscopic homogenity, very large specimens would be required. This would mean that the forces needed to produce measurable deflections and thus enable moduli to be calculated, would be large and difficult to obtain in the laboratory. In addition, there would be doubt as to the applicability of the results to specimens with fibres of two or more orders of magnitude smaller. It was therefore decided to develop a method of making ordered arrays of fibres of any desired concentration which could be infiltrated with resin without the use of pressure.

More than 45 laminates with unidirectional reinforcement were prepared and examined. Specimens were machined from each laminate with axes at different angles to the fibres and their torsional moduli and damping factor determined using a torsional pendulum. The determinations were made over a temperature range which included the glass transition point of the resin (65°C). After the mechanical properties had been measured, the specimens were cut up; fibre concentrations were determined on the cylindrical centre section and a microscopic examination made on the residue. The results obtained were then compared with those predicted by using the formulae postulated by three previous workers in the field.

3. WORK CARRIED OUT AND RESULTS OBTAINED

3.1. Manufacture of the fibres for reinforcement

Fibres of pure vitreous silica approximately 90μ in diameter were drawn from 3 mm diameter rods by heating in an oxygen/coal gas flame. If a finish was required on the fibre surface, it was passed through a solution of 10% A1100 in distilled water. (A1100 is the Union Carbide code for γ-aminopropyl triethoxy silane.)

3.2. Preparing the fibre mat

The fibres were wound on to an accurately turned cylinder on a lathe using the lead screw to space the filaments by the required amount. The cylinder was 150 mm in diameter and 300 mm long, enabling four bands of fibres of about 65 mm width to be wound on it. Longitudinal strips of 25 mm wide adhesive tape were secured, sticky side up, to the drum in three places around its circumference before winding so that the fibres could stick to it and retain their lateral displacement. After completing the winding a second strip of adhesive tape sticky side down was placed over the first in each case dividing the fibres into three equal lengths along the circumference. The entire "mat" could then be removed from the drum by cutting down the centre of one of the strips giving a band approximately 250 mm wide by 450 mm long divided into three parts. This large mat was then cut into pieces 57 mm wide and 150 mm long ready for stacking in an array.

3.3. Moulding the composites

The mould used to cast the specimens is shown in Fig.1. This was used for unidirectional specimens although other moulds were produced to manufacture specimens with crossplied reinforcements. The end pieces of the mould were accurately ground to be 57±0·025 mm long. Fibre mats were cut to this width on a simple cutter and stacked in the mould with brass or steel shims of the correct thickness at each end to space the layers apart. After inserting the end pieces the shims were strained slowly between the grips of a tensile testing machine in order to pull the fibres tight and align them. When full alignment was achieved the end pieces were clamped tight and the array was ready for impregnating with resin.

The spacings achieved by this method were not entirely perfect. Figs.2 and 3 show the best and worst achieved. However, compared with commercial material (Fig.4) there are several advantages. The fibres retained their parallelism throughout their length and there were very few fibre to fibre contacts, the dispersion being generally good. The casts were approximately 1 cm thick. Twenty layers of fibres were used in the lower concentrations; 40 or more layers as necessary for higher concentrations.

The fibre content of Cast 30 was disappointingly low and so a different method was used to prepare the remaining "maximum concentration" casts. These were made by packing a cylindrical mould as tightly as possible with fibres. The cast was then infiltrated with resin.

3.4. Preparation of the epoxy resin

The epoxy resin used to manufacture the specimens was Shell RXE11 with Shell Epikure RXE11 hardener which is a mixed anhydride. In order to bring the glass transition temperature to a lower value than normal, for ease in experimentation, equal weights of an aliphatic epoxy resin Araldite X83/219 were added to the Shell resin before curing. In this way the glass transition temperature (T_g) was lowered from about 125°C to 65°C and the system could be simply studied in the laboratory. Full details of the preparation of the various casts are shown in Table 1.

3.5. Preparation of control specimens

It is possible that variation in the chemical compositions of the resins and changes in the curing cycle could produce variability in the samples which might mask the effects of fibre reinforcement alignment and fibre concentration. Control samples were therefore made from the unreinforced part of each cast, being the strip about 15 mm wide on each side of the 57 mm central band. The results obtained are shown graphically in Fig.7 and tabulated in Table 2.

3.6. Design of the test specimen

In order to simplify the calculation of torsional modulus, it was decided to use test pieces of circular cross-section. The stress acting on any annulus could be assumed to be reasonably uniform although there would of course be variation in a radial direction. Test pieces were cut from the above casts at angles of 0°, 30°, 45°, 60° and 90° to the fibre axis. This enabled the moduli at various angles to the fibre axis to be determined.

Test pieces were machined to the shape shown in Fig.5. The splines at each end of the specimens engaged with corresponding pieces in the spring loaded grips which are shown in Fig.6. These grips were designed to hold the specimen in shear while allowing for expansion and contraction during the heating cycle.

3.7. Measuring the torsional moduli and damping factors

These tests were performed with a torsion pendulum of conventional design, the sample being immersed in a temperature controlled oil bath. The oscillations of the pendulum were recorded by means of a suitable recorder. The frequency of oscillation was maintained as nearly as possible to 1 Hertz by varying the inertia of the pendulum when necessary.

From the recording the torsional modulus, 'G' and the damping factor, "tan δ" were measured. The maximum deflection of the trace was never more than 100 mm at an optical lever length of 1 metre. The angle of torsion on a 28 mm long test piece was therefore only 0·05 radian. Determinations were made at various sample temperatures between 20°C and 120°C.

3.8. Measurement of fibre concentration

After the mechanical measurements had been made the samples were cut up and the cylindrical section used to determine fibre concentration. These were calculated from the determinations of density and by ashing the composite. The results are set out in Table 3.

3.9. Effect of amino-silane finish on the α peak

A test to determine the effect of the amino-silane finish on the position of the α peak was carried out. A standard 100:100:75 resin/hardener mixture was cast in four identical moulds and 0·8%, 0·5%, 0·3% and 0·0% of A1100 silane added to the four moulds respectively. All four were then cured for 16 hours at 116°C. The test results are plotted in Fig.9.

3.10. Effect of specimen length on shear modulus

To test the effect of specimen length on the measured values of modulus Cast 17 was used. Specimens were cut with standard end grips but with different test lengths, namely 55 mm and 40 mm. A 40 mm long sample was also cut from a control specimen. Shear modulus was measured at 25°C and 100°C and results are given in Table 4.

4. DISCUSSION OF RESULTS

4.1. Fibre concentration

An examination of Table 3 indicates that the two methods of determination of fibre concentration agreed to within 2% at the higher concentrations but with less accuracy at the very low concentrations. A comparison of Tables 1 and 3 shows that the fibre concentration which was achieved was generally fairly near to the design aim.

4.2. Results of mechanical tests on the control samples

4.2.1. Variability

An examination of the results in Table 2 shows some variability in the results of the five casts examined. The high values of tan δ achieved on Cast 13 are probably attributable to the fact that this cast was submitted to a less effective curing cycle than the remainder. The variability exhibited by the other casts is less easy to explain, however the results indicate that Casts 18 and 20 which received the most prolonged curing cycle gave the least variable results. Another source of variability could be the fact that varying proportions of volatile components in the resin boiled off during the vacuum treatment. For this reason the procedure which was followed of using as a control for each cast an unreinforced resin sample from the same cast, was clearly correct.

4.2.2. Effect of the state of cure on resin properties

Casts 29 to 43 were post-cured at about 155°C. This is some 20°C higher than the earlier casts. Comparison of the controls from these casts with those of earlier ones shows no appreciable change in the position of the α peak. It is however clear that the resin mixture is probably not fully cured chemically and that the addition of more hardener would increase the cure and thus the temperature at which the α transition occurs. This has an important effect when amino-silane coupling agents are used as will be discussed later.

The effect of increasing the amount of hardener is shown in Casts 35 and 37. (Fig.8) Cast 35 was prepared from proportions of 100:100:75 of the two resins and hardener whilst Cast 37 contained proportions of 100:100:105. The α peak for Cast 35 was at about 65°C whilst that for Cast 37 was at 76°C. The lower figure is within the normal region for this mixture when cured; the higher figure for Cast 37 is undoubtedly due to increased crosslinking. It should be noted that both specimens were cured under the same temperature conditions.

4.3. Theory

4.3.1. The elastic compliance tensor for arbitrary fibre direction

The symmetry in a unidirectionally fibre reinforced specimen with hexagonal packing is that of transverse isotropy with 5 elastic constants. Assuming that the 1 - axis lies along the fibres, then the elastic stiffnesses are, in tensor form:

$$\begin{matrix} C_{11} & C_{12} & C_{12} \\ C_{12} & C_{22} & C_{23} \\ C_{22} & C_{23} & C_{22}-\frac{1}{2}(C_{22}-C_{23}) \\ & & C_{55} \\ & & & C_{55} \end{matrix}$$

where engineering strains are used.

The elastic compliance tensor is:

$$\begin{matrix} S_{11} & S_{12} & S_{12} \\ S_{12} & S_{22} & S_{23} \\ S_{12} & S_{23} & S_{22}-2(S_{22}-S_{23}) \\ & & S_{55} \\ & & & S_{55} \end{matrix}$$

therefore:

$$E_1 = \frac{1}{S_{11}}$$

$$E_2 = \frac{1}{S_{22}}$$

$$\nu_{13} = \nu_{12} = -S_{12}/S_{11}$$

$$\nu_{21} = \nu_{31} = -S_{12}/S_{22}$$

$$\nu_{23} = \nu_{32} = -S_{23}/S_{22}$$

and $\nu_{21} E_1 = \nu_{12} E_2$

For torsion around the symmetry axis Hearmon [9] shows that

$$G = \frac{2}{S_{55} + S_{66}} = \frac{1}{S_{55}} \quad \text{(Eqn 1)}$$

for general torsion of a cylinder cut at an angle to the symmetry axis Voigt[10] shows:

$$G = \frac{2}{S^1_{55} + S^1_{66}} \quad \text{(free torsion) . . . (Eqn 2)}$$

$$G = \frac{2}{S^1_{55} + S^1_{66} - (S^1_{55}{}^2 + S^1_{66}{}^2)/S^1_{11}} \quad \text{(pure torsion)}$$

In the latter case the bending associated with torsion is prevented. Now the general tensor for the fibre-reinforced material is:

$$\begin{array}{cccccc}
S^1_{11} & S^1_{11} & S^1_{13} & 0 & 0 & S^1_{16} \\
S^1_{12} & S^1_{22} & S^1_{23} & 0 & 0 & S^1_{26} \\
S^1_{13} & S^1_{23} & S^1_{22} & 0 & 0 & S^1_{36} \\
0 & 0 & 0 & S^1_{44} & S^1_{45} & 0 \\
0 & 0 & 0 & S^1_{45} & S^1_{55} & 0 \\
S^1_{16} & S^1_{26} & S^1_{36} & 0 & 0 & S^1_{66}
\end{array}$$

where the S^1_{ij} are obtained from the S_{ij} by rotation of axes 1 and 2 about the 3 - axis (Hearmon 4.4).
G becomes:

$$2/\left[2n^2(S_{22}-S_{23}) + m^2S_{55} + 4m^2n^2(S_{11} - 2S_{12} + S_{22}) \right.$$

$$\left. +(m^2-n^2)^2S_{55} - \left[\frac{m^3n\,(2S_{12} - 2S_{11} + S_{55}) + mn^3\,(2S_{22} - 2S_{12} - S_{55})}{m^4S_{11} + m^2n^2(2S_{12} + S_{55}) + n^4S_{22}} \right]^2 \right]$$

where $m = \phi$

$n = \phi$

where ϕ is the angle between the symmetry axis and transformed axis; the term in square brackets being zero if free torsion is allowed.

Therefore, if the elastic constants are known for the unidirectional case then the shear modulus for a sample cut at any angle can be predicted.

In the experimental arrangement used the mounting of the specimen was such that bending was prevented and therefore the appropriate shear modulus is that for the pure torsion (restricted bending) case. G0, G30, G45, G60 and G90 have been calculated for comparison with experimental results.

If further the assumption is made that complex quantities can be used in the equations then $G^* = G^1 + G^{11}$, where G^1 is the measured modulus and G^{11}, where G^1 is the measured modulus and $G^{11}/G^1 = \tan\delta$ can be calculated from the tensor of complex compliances S^*_{ij}. The validity of this approach is discussed by Biot (11) and Rogers (12).

4.3.2. Calculation of the elastic compliance tensor (S_{ij})

The S_{ij} values have been calculated from three different published formulae. The simplest is the theory of Whitney and Riley (3) who assume a composite unit cell of cylindrical form and apply classical elasticity theory to produce a solution in closed form. This is particularly convenient for calculation since it permits the use of a computer programme which only requires input data relating to the elastic constants of fibres and matrix separately and the fibre concentration.

The second theory used is that of Savin and Van Fo Fy (4) who give approximate formulae, derived from their more detailed analysis, for the S_{ij}. The third souce of S_{ij} values is from the bounds on elastic moduli derived by Hashin (13) and by Hill (12). The validity of the three different approaches and their comparison with measured results is discussed below.

4.3.2.1. Whitney-Riley model

Whitney and Riley calculate a solution which is almost exact for a single composite cylinder. (Cylinder of matrix material concentric with reinforcing fibre.)

They make one assumption in their derivation however, which is that the transverse Poisson's ration ν_{23} is a linear combination of the Poisson's ratios of fibre and matrix in proportion to fibre concentration. Their further assumption is, of course, that the

single composite cylinder is representative of an array of closely packed cylinders.

Calculation of the stress produced by stretching a uniform plate containing an inserted elastic disc shows that the effect of the disc will become noticeable at about 3 radii from its centre. For hexagonal close packed fibres this amounts to about 10% by volume.

The Whitney-Riley theory, assuming that ν_{23} is adequately given by the linear approximation referred to above, should therefore be valid up to about 10% by volume of fibre but progressively fail thereafter.

4.3.2.2. Van Fo Fy and Savin formula

Van Fo Fy and Savin set up the equations of equilibrium for fibres in a hexagonal array using the Muskhelishvili method. They chose Weierstrass elliptic functions, which have the required symmetry of the hexagonal lattice, to construct a solution and give the conditions of compatibility for the matrix fibre boundary.

In theory this method of solution with the addition of the solution of the problem of tension-compression parallel to the fibres should yield exact solutions in series for the stresses and displacements in the body. They quote, however, only an approximate solution, accurate to 15% and give the S_{ij} in terms of fibre and matrix moduli and the fibre concentration. Their expressions for S_{55}, and S_{11} and S_{12} coincide with those given by Whitney and Riley but those given for S_{22} and S_{23} differ considerably. Since it is these latter which determine the shear properties for off-axis deformations the Van Fo Fy and Savin theory should give better results than Whitney-Riley.

4.3.2.3. Hashin - Hill bounds

Hashin [13] gives bounds on the plane strain bulk modulus, on G_{23} and on G_{12}, while Hill gives bounds on ν_{12} and on E_1. In both cases these bounds are given for arbitrary transverse phase geometry and therefore should hold whether the packing is hexagonal or not.

Values of S_{ij} for both upper and lower bounds were calculated from these formulae and used to predict upper and lower bounds for the shear moduli at angles to the fibres.

In all three sets of formulae it is possible to substitute complex quantities for the elastic moduli of fibre and matrix and therefore to predict the modulus and damping of the composite. This has been done in deriving the curves. The validity of this is discussed later.

4.4. Comparision of theoretical values with test results

4.4.1. Modulus, glassy region (Figs.10 to 14)

At fibre concentration up to 10%, agreement between theory and experiment appears to be satisfactory. Both the simple theory of Whitney-Riley and the Van Fo Fy - Savin approximation give similar results though differences start to appear as the angle of the fibres to the specimen axis increases towards 90° and brings in a larger proportion of the terms S_{22} and S_{23}. The Hashin - Hill lower bound coincides everywhere with the Van Fo Fy - Savin value. Thus, as expected for fibre concentrations where the stress field from one fibre cannot appreciably affect the next fibre the composite cylinder approximation is quite accurate.

For fibre concentrations of greater than 10% however the simple theories do not predict the shear modulus accurately except at 0^0 and 90^0. The Whitney - Riley value is in error for the 90^0 case when the concentration is over 30%, and in all cases gives higher values than the other two theories. For the 30^0, 45^0 and 60^0 specimens the measured modulus is greater than either the Whitney - Riley or Van Fo Fy - Savin predicted values as soon as the fibre concentration rises above 10% although the figures still lie between the Hashin - Hill bounds.

4.4.2. Rubbery region (Figs.15 to 19)

In this region the differences between experiment and theory are even more marked. For all fibre concentrations there is poor agreement between measured and calculated values of the shear modulus.

The difference amounts to a factor of about 1·5 at very low concentrations for the 0^0 orientation rising to 3 at 40% concentration. In all cases the measured modulus was the greater by this factor, which effectively rules out the possibility of the fibres slipping in the resin, or otherwise being ineffective.

As the orientation of the fibres changes towards 90^0 the differences between theory and experiment are reduced considerably, being noticeable only at the higher concentrations while there is agreement at the low concentrations.

4.4.3. Damping, glassy region (Figs.10 to 14)

For specimens with nearly rigid fibres in a more compliant matrix ($G_F/G_M \sim 60$) it would be expected that most of the energy absorbed in oscillations would be in the visco-elastic matrix material and hence that the tan δ curves for the composite should always lie near to those for the pure matrix material. In general this appears to be the case, the control curves acting as good approximations to the curves for the reinforced material at all fibre angles, up to a concentration of about 10%. It is still true up to 40% fibre for the 0^0 and 90^0 cases but it is very far from being true for the 30^0, 45^0 and 60^0 cases at the higher concentrations.

Theory would lead one to expect a lowering of the value of tanδ for the off axis cases and this is shown in the curves drawn for the various theories. The amount of shift is however much greater than expected.

4.5. Possible reasons for the anomalies

The experimental anomalies at 30^0, 45^0 and 60^0 for high fibre concentrations could arise from several causes:

(1) excitation of the bending mode during testing

(2) invalidity of the assumption that $S_{12} = S_{21}$

(3) invalidity of other assumptions

(4) shift of the α peak to higher temperatures

(5) inapplicability of the Voigt relation (Eqn.2)

These are discussed separately.

4.5.1. Excitation of the bending mode during testing

With samples cut at angles to the fibre axis it is difficult not to excite the bending mode which can naturally occur with asymmetric specimens. In some cases these oscillations were apparent but by no means in all and it could not therefore account for the fact that at all temperatures in casts 18 and 20 the value of tan δ for the 30°, 45° and 60° cases is well below the control value. A full analysis of the modes of vibration and their interplay needs to be done, but at first sight one might expect tan δ to increase if energy is being absorbed in an additional mode, rather than to decrease.

4.5.2. Invalidity of the assumption that $S_{12} = S_{21}$

It has been assumed that $S_{12} = S_{21}$. Rogers and Pipkin [12] point out however that this assumption in a time dependent system implicitly assumes the validity of the Onsager reciprocal relations and therefore needs experimental verification.

For 0° and 90° S_{12} and S_{21} occur as a sum but for other angles they do not and can play larger or smaller parts depending on the angle. Hearmon[9] notes a failure of the relation in some experiments on wood but suggests that experimental errors or inhomogeneities may be responsible. Computed results for S_{21} varying from $0{\cdot}5\ S_{12}$ to $2S_{12}$ show only small changes in tan δ(Table 5). It is therefore concluded that this cannot be the cause of the anomalies.

4.5.3. Invalidity of other assumptions

The anomalies in the calculated results may also be due to the assumptions made in choosing input data for the programmes.

These were (a) Poisson's ratio for the resin = 0·35

(b) The glass transition for Young's modulus (E) occurs at the same temperature as it does in shear.

The effect of the first assumption is small as may be seen from the results in Table 6, calculated for Cast 20 at 45°C and 50°C using E/G ratios of 2·7, 2·8 and 2·9 corresponding to Poisson's ratios of 0·35, 0·4 and 0·45 respectively.

G_o is unaffected by changes in Poisson's ratio since it is independent of it.

It is clear that the changes in the shear modulus as a result of changing Poisson's ratio are not sufficient to account for the anomalies found.

It would be of value to have a direct measurement of Young's modulus, the bulk modulus or Poisson's ratio at the temperature and frequency of the measured shear modulus but this is not an easy task if accuracy comparable with that possible in torsion is desired.

The majority of methods (see e.g. Neilson [15]) use forced oscillations or resonance at a considerably higher frequency than that used in this work for shear measurements. This would shift the relaxation peak an unknown amount and make the use of such results questionable. An attempt has been made to measure Young's modulus and damping in bending at 1 Hertz but unsatisfactory results were obtained.

There is some evidence (Kono [16]) that the positions of the glass/rubber transition temperatures in shear and in bulk differ but the problem has been very little studied.

4.5.4. Shift of α peak

Examination of the α-transition in its entirety shows that there is a lowering of the tan δ peak in the glassy region accompanied by a general shift of the transition to a higher temperature. This could have several causes but the most likely are

(1) a change of the effective glass transition temperature by increased cross linking in the fibre filled material

(2) a physical change in this temperature by reason of the mechanical interaction between fibres and resin

It would seem that both mechanisms are playing a part as will now be demonstrated.

4.5.4.1. Cross linking of the resin

It was mentioned previously that although the resin system could not be further cured by more heat treatment it was not fully chemically cured. In preparing most specimens the fibre was drawn through a bath of 10% A1100 in water and this deposited a fairly large (but undetermined) amount of silane finish on the fibre. Sterman and Marsden [17] have shown that the weight per cent of silane required is given by

$$\frac{\text{surface area of 100 grams of filler}}{\text{area covered by 1 gram silane}}$$

and for the present system this is approximately 0·6 weight per cent. In section 3.9 it has been shown that an addition of this amount of silane to the same resin system will give an upward shift in the glass transition temperature of 4° to 5°C and this is the order of the shifts found in Casts 18, 20, 30 etc. which use A1100.

By contrast no finish was used in Cast 29 and the glass transition temperatures are coincident, within experimental error, with the control values (Figs.20 to 26). It seems clear therefore that the shift in glass transition temperature between control and filled systems could be due to the effect of the silane finish.

4.5.4.2. Interaction between fibres and resin

The results indicate another possible reason for a shift of the α transition. Casts 33 and 42 were made without silane yet a clear shift of the α transition relative to the control samples is evident in both these casts (Figs.27 and 28). These two casts contained higher fibre concentrations and it appears that this shifts the α-peak, broadens and flattens it. Explanations for this phenomenon in casts with a higher fibre concentration are considered below.

4.5.5. Factors in casts with higher fibre concentrations which could affect the α transition

4.5.5.1. Artefacts

Slippage of fibres in the resin during the torsion test could absorb energy and raise the level of tan δ. However it is difficult to see why this should not lead also to a modulus much less than the theoretical value instead of greater. Furthermore it should also occur in the glassy region, yet tan δ is lower in this region than the control value.

4.5.5.2. Shape or type of sample

It is not clear how this could affect tan δ which is a dimensionless quantity although it could conceivably alter the measured modulus values.

To test the effect of specimen length on the measured values of modulus Cast 17 was used, specimens being cut with the standard end-grips but different test lengths. The results obtained are tabulated in Table 4.

The modulus values for the control are quite comparable with those for a normal 28 mm specimen and the calculated moduli for the glassy state (25°C) agree reasonably with the measured values although they are a trifle low in the case of the long specimens. In all cases however the predicted rubbery modulus is low as compared with the measured one, exactly as is the case with the normal specimens.

4.5.5.3. Secondary relaxation peak

The change in shape of the α peak in the highly reinforced samples could be explained if there were a high temperature absorption peak in addition to the normal one for the flexibilised resin at 65°C. Such a peak could be the usual one for epoxy resins at about 120 - 140°C but although it is conceivable that this might appear as a result of cross-linkage between resin and the surface active agent (the silane finish on the glass) it is impossible to see how this mechanism could exist when no finish is present.

4.5.5.4. Constraint of fibres on resin

Thermal expansion could result in compressive stress of up to 70 bar in the resin assuming perfect bonding of fibres and resin. The resultant restriction of free volume of the resin could increase Tg by several degrees (O'Reilly [18]) but it is unlikely that it could account for the very large shifts of tan δ found, for example, in Casts 34, 42 and 43 (Figs.27, 28 and 29).

4.5.5.5. Fibre-fibre contact

We have assumed so far the idealised model of a uniform dispersion of fibres. However it is possible that at high fibre concentrations appreciable numbers of fibres may make contact with each other and, during deformation, cause a frictional contribution to the damping.

Consider the equation of motion of the torsional system

$$I\ddot{\theta} + \kappa\dot{\theta} + G\theta = 0$$

The solution for free oscillations is

$$\theta = \exp(-\kappa t/2I)(A \cos wt + B \sin wt)$$

where $w^2 = \frac{4GI - \kappa^2}{4I^2}$

The relations $\tan\delta = \lambda/\pi$, $\lambda = \frac{\kappa}{2I}$ are used and λ measured directly from the observed damping curve. There are errors in using this method (Struick [19]) but they are not large. Now suppose that the frictional damping term κ contains a constant factor k

then $\tan\delta = \frac{\kappa' + k}{2I\pi}$

and the values of $\tan\delta$ as a function of temperature could differ from those expected theoretically by a constant factor. The effect will be much larger in the rubber region where I is small than it is in the glassy region where I is about 300 times greater. Comparisons between derived and experimental values of $\tan\delta$ are given in Table 7.

The inertia terms in the rubbery region were constant for all three of these casts so that it is permissible to use the difference of $\tan\delta$ rather than the difference of κ.

Within the limits of experimental accuracy of $\tan\delta$ the differences do appear to be constant, which is encouraging confirmation of the theory particularly considering the decade difference of $\tan\delta$ between 85°C and 105°C. The exception appears to be Cast 43 where the differences become greater at the lower temperatures. However if the theoretical curve for $\tan\delta$ for this case is shifted to higher temperatures by the amount of the shift found in the glassy region then the differences become more regular. In considering the reason for these effects on $\tan\delta$ it is supposed that it is the friction between fibres rather than fibre slippage which is important on the grounds that slippage of fibres in the resin should be more likely when no finish is present than when the fibres are bonded to the resin. Yet the values of $\tan\delta$ for Cast 43 at high temperatures lie above those for the (dry) Cast 42. Shift of the curves for Cast 42 along the temperature axis in fact give reasonable superposition on to those for Cast 43.

Thus the $\tan\delta$ curve in the rubbery region would seem to be related to that for the control resin (theoretical curve) by two factors:

(a) The shift of Tg to a higher temperature caused by the chemical effect of the surface active agent (A1100)

(b) The increase of $\tan\delta$ by frictional work between fibres.

5. A THEORY OF FRACTURE OF FIBRE REINFORCED VISCOELASTIC MATERIALS

5.1. Concepts of fracture

5.1.1. The meanings of brittle and tough

Toughness is a remarkably ill-defined word with many interpretations of its meaning. Intuitively it is felt that a material which withstands a hammer blow is tough; whereas one that shatters under such treatment is brittle. This view, upon refinement, leads to the various impact tests such as Izod and Charpy.

A second definition comes from the load-extension curve. If this rises in a more or less straight line to fracture such as in the testing of glass, the material is brittle. If there is a yield point and a fair measure of extension after the point, as in mild steel, the material is tough. Under this definition rubber is a tough material, as are most plastics above their glass transition. However, both temperature and rate of strain are very important with polymeric materials and both impact and stress-strain methods can give highly erroneous results unless this is taken into account.

5.1.2. Modes of failure

In many applications it is the mode of failure which is important and for this purpose a study of the fracture process has proved profitable. This has led to the modifications of the Griffith crack theory for brittle solids to take into account plastic and other work done in enlarging a crack in the material. In metals this extension was made by Orowan [21] and by Irwin [22] and in rubber by Rivlin and Thomas [23]. The concept is of energy balance between the elastic energy released as a crack extends and that used in creating new surfaces, in plastic work or in irreversible deformation processes. If the former exceeds a level known as the characteristic surface energy or crack extension force (Irwin) then the crack becomes unstable and fracture occurs. This theory has been highly successful in many fields of materials and will be adopted here.

5.1.3. Thermosets

Thermosets generally, are brittle rather than tough materials although the development of polyester and epoxy resins has given industry materials which are less brittle than the old thermosets, but which are still not capable of absorbing energy very rapidly nor of sustaining flaws under tensile loading. An indication of the relative toughness of plastics and metals is given in Tables 7 and 8.

It is clear that in comparison with the more common metals thermosetting resins do not have very great toughness as defined by impact strength and surface energy determinations and even the incorporation of reinforcement does not improve the figure by more than a factor of 10.

5.1.4. Previous work

Various authors have studied the effect of type of hardener, its amount and the temperature of curing on the mechanical properties of epoxy resins. Lewis and Ramsey [26] using Epon 828 and diethylene triamine found fracture energy (area under stress-strain curve) increased with curing by a factor of about 4. This is in accordance with common experience that a room temperature amine-cured epoxy is much more brittle than one cured at a higher temperature. Mostovoy

and Ripling [27] confirm this using a measure of $G_c = (P_c^2/2b)\frac{\delta C}{\delta a}$ where "P_c" is the applied load at the instant of fast crack extension, "b" specimen thickness, "C" specimen compliance, and "a" the crack length. They used DER 332 and TEPA and showed that G_o, the characteristic surface energy increased with increased post cure temperature and also with increasing amounts of TEPA until a limit was reached.

Burhans et al[28] have shown that decreasing the distance between "active sites" (the carbon atoms furthest from the ether linkage in epoxies) increases both modulus and strength but this is generally at the expense of toughness. Conversely, toughened epoxies can be made by incorporating long chain molecules of either resin or hardener into the cross linked network. Thus the long chain aliphatic epoxy Araldite X83/219 imparts toughness to the systems in which it is mixed and the same effect is found by using dodecynyl succinic acid as hardener with a standard bisphenol A or epoxy novolac resin system. There is considerable evidence that the curing of epoxy resins may be excessive if maximum toughness is required. Lewis and Ramsey found that cure at 60°C for four hours followed by a short post-cure at 190°C gave the best results, and it is probable that this left an appreciable number of groups unreacted. It can be seen that resins are no exception to the general rule found in metals that high strength gives low toughness (or in other words poor resistance to crack propagation) and vice versa. Thus the strongest steels are the most brittle and the same is true of resins. (Vincent [36], Bobalek and Evans [37]).

5.1.5. Effect of fibre reinforcement

Fibre reinforcement of thermosetting resins is claimed to combine strength and toughness. In order to investigate this claim the mode of failure of a fibre reinforced resin must be considered in some detail taking into account the way in which elastic strain energy can propagate through the material and in what way it can be dissipated.

5.2. Theoretical considerations of fracture in a fibre-reinforced resin under tension

As a tensile specimen with unidirectionally oriented fibres is loaded elastic energy is stored in the fibres and the resin while a certain amount is also dissipated in the resin (since it is viscoelastic). At a certain strain either the resin will fail from some stress concentration such as a bubble or one fibre will break. The result will be similar in the two cases in that

(a) the remainder of the fibres will carry a slightly increased load

and

(b) a stress concentration will exist at the tip of the crack and will therefore increase the likelihood of its spreading.

5.2.1. Energy at fracture site

Three conditions are possible: either the crack will spread under the applied load, or a new crack will develop, or the system will still be stable. To ascertain which will occur it is necessary to calculate whether the strain energy released by spreading of the crack (including the breaking of fibres) is sufficient to supply the needs of the new surfaces, and of

viscoelastic and frictional work. The fact that the fibres may not have a uniform strength or breaking strain, but a variable one distributed about a mean value must also be taken into account. In addition it is unlikely that all fibres are equally well aligned or that they are equally strained; this will also produce variability.

5.2.2. The proposed model

In setting up the proposed model three assumptions have been made.

5.2.2.1. Assumption 1

It is assumed that when one fibre breaks the disturbance in local stress extends to nearest neighbours only and for a length on either side of the break equal to the elastic transfer length (defined below).

5.2.2.2. Assumption 2

It is also assumed following Kelly (29) and Cox (30), that the shear stress in the resin at the surface of the broken fibre, at a distance x from the broken end is

$$\tau(x) = \sqrt{\frac{E_f \; G_m}{2\ell_n \, R/r_f}} \cdot \frac{\varepsilon \sinh \beta \, (\ell/2 - x)}{\cosh \beta \, \ell/2} \quad \ldots\ldots\ldots \text{(i)}$$

where E_f is Young's modulus for the fibre

G_m is shear modulus for the resin

ε overall strain in the composite

$2R$ mean separation of fibres laterally

r_f fibre radius

$\ell/2$ elastic transfer length

$$\beta = {}^{1}/_{r_f} \sqrt{\frac{2G_m}{E_f \, \ell_n \, R/r_f}}$$

Together with this expression for the shear stress in the matrix the stress in the broken fibre at a distance x from the free end is taken to be

$$\sigma_{bf} = E_f \, \varepsilon \left[1 - \frac{\cosh \beta \, (\ell/2 - x)}{\cosh \beta \, \ell/2}\right] \quad \ldots\ldots \text{(ii)}$$

$$\text{for } o < x < \ell/2$$

It is clear that this expression can never equal the stress in the unbroken fibres unless ℓ is very large.

However, if $\beta\ell/2 = 2$ the stress at $x = \ell/2$ will reach 70% of the unbroken stress, if $\beta\ell/2 = 3$ it reaches 90%. We therefore <u>define</u> $\ell/2$ the <u>elastic transfer length</u> to be equal to $3/\beta$ ..... (iii)

5.2.2.3. <u>Assumption 3</u>

The shear stress in the resin at point (r,x) is taken to be:

$$\tau(r,x) = r_{f/r}\,\tau(r_f, x)$$

$$= \sqrt{\frac{E_f\, G_m}{2\,\ell_n\, R/r_f}} \cdot \frac{\varepsilon\, r_f \sinh \beta\,(\ell/2 - x)}{r \cosh \beta\, \ell/2}$$

Hence the load in an adjacent fibre, P, is related to this shear stress by:

$$\frac{dP}{dx} = 2\pi\, r_f\, \tau_f$$

Consider the stress $\sigma_{af} = \frac{P}{\pi r_f^2}$ at an adjacent fibre distant 2R from the broken one. Then:

$$\sigma_{af} = \frac{1}{\pi r_f^2}\, 2\pi\, r_f \int \tau\,(2R,x)dx$$

$$= 2/r_f \sqrt{\frac{E_f\, G_m}{2\ell_n\, R/r_f}} \cdot \frac{\varepsilon\, r_f}{\cosh \beta\, \ell/2} \cdot \frac{\cosh \beta\,(\ell/2 - x)}{2\beta R} + C$$

The constant C is found by equating σ_{af} to 0 at $x = \ell/2$ since we are only interested in the <u>incremental</u> stress

$$\therefore\ 0 = C + \frac{\varepsilon}{\beta R} \sqrt{\frac{E_f\, G_m}{2\ell_n\, R/r_f}} \cdot \frac{1}{\cosh \beta\, \ell/2}$$

and

$$\sigma_{af} = \frac{\varepsilon}{\beta R \cosh \beta\, \ell/2} \sqrt{\frac{E_f\, G_m}{2\ell_n\, R/r_f}} \left[\cosh \beta \left(\ell/2 - x\right) - 1\right]$$

But

$$\beta = \frac{1}{r_f} \sqrt{\frac{2\, G_m}{E_f\, \ell_n\, R/r_f}}$$

$$\therefore \quad \sigma_{af} = \varepsilon \frac{r_f}{R} \cdot E_{f/2} \frac{[\cosh \beta\ (\ell/2-x)-1]}{\cosh \beta\ \ell/2}$$

$$= \sigma_f \left[\frac{r_f}{2R} \cdot \frac{\cosh \beta\ (\ell/2-x)-1}{\cosh \beta\ \ell/2}\right] \qquad \ldots\ldots \qquad (iv)$$

At $x = 0$ this has the value

$$\sigma_{a_f}(0) = \sigma_f \left[\frac{r_f}{2R}\left(1 - \frac{1}{\cosh \beta\ \ell/2}\right)\right]$$

But, by definition, $\beta\ell/2 = 3$, hence $\cosh \beta\ell/2 = 10$

$$\sigma_{a_f}(0) = \sigma_f \left(0{\cdot}45\ r_{f/R}\right) \qquad \ldots\ldots \qquad (v)$$

The energy released when a fibre breaks can now be calculated and it can be determined whether the stress on an adjacent fibre will be sufficient to break it.

5.2.3. Energy changes during fracture

Only the "transfer zone" mentioned above is being considered, i.e. the energy available for spreading of the crack comes only from a re-arrangement of the stresses in the transfer zone and not from any relaxation of stress outside. The elastic strain energy in the zone before fibre fracture is $\frac{1}{2}\sigma_c\ \varepsilon\pi(R)^2\ell = E_c$. After fracture it is the sum of E_{bf} (the strain energy in the two broken portions of the fibres) + E_m (the energy in the matrix material), and the energy released on fibre fracture is therefore $E_c - E_{bf} - E_m$. Expressions for E_{bf} and E_m are developed below.

It is assumed that this energy goes

(1) to increase the strain energy of the six adjacent fibres
(2) to supply the surface energy of the new surfaces created
(3) to supply the heat and other energy absorbed during fracture

5.2.4. Energy expressions

5.2.4.1. Energy in the broken fibre

$$E_{bf} = 2 \times \frac{\pi r_f^2}{2\,E_f} \int_0^{\ell/2} \sigma_{bf}^{\ 2}\ dx$$

$$= \frac{\pi r_f^2}{E_f} E_f^2 \varepsilon^2 \int_0^{\ell/2} \left[1 - \frac{\cosh \beta \left(\ell/2 - x\right)}{\cosh \beta \ell/2} \right]^2 dx$$

$$= \pi r_f^2 \varepsilon^2 E_f \left[\ell/2 - 2/\beta \tanh \beta \ell/2 + \left(\ell/4 + \frac{\sinh \beta \ell}{4\beta} \right) \operatorname{sech}^2 \frac{\beta \ell}{2} \right] \quad \ldots \quad (vi)$$

5.2.4.4. Energy in the matrix material

$$E_m = 2 \times \tfrac{1}{2} \int_{r_f}^{R} \int_0^{\ell/2} \frac{\tau (rx)^2}{G_m} 2\pi r \, dr \, dx$$

$$= \frac{2\pi}{G_m} K^2 \int_{r_f}^{R} \frac{dr}{r} \int_0^{\ell/2} \sinh^2 \beta \left(\ell/2 - x\right) dx$$

where $K = \sqrt{\frac{E_f G_m}{2 \ell_n R/r_f}} \cdot \frac{r_f \varepsilon}{\cosh \beta \ell/2}$

$$\therefore \quad E_m = \frac{2\pi K^2}{G_m} \ell_n R/r_f \int_0^{\ell/2} \tfrac{1}{2} \left(\cosh 2\beta \left(\ell/2 - x \right) - 1 \right) dx$$

$$= \frac{2\pi}{G_m} K^2 \ell_n R/r_f \left[\frac{\sinh \beta \ell}{4\beta} - \ell/4 \right]$$

$$\text{ie } E_m = \frac{\pi E_f r_f^2 \varepsilon^2}{\cosh^2 \beta \ell/2} \left[\frac{\sinh \beta \ell}{4\beta} - \ell/4 \right] \quad \ldots \quad (vii)$$

5.2.4.5. Energy in adjacent fibres

$$E_{af} = 6 \times 2\pi r_f^2 \times \tfrac{1}{2} \int_0^{\ell/2} \frac{\sigma_{af}^2}{E_f} dx$$

$$= \frac{6 \pi r_f^2 \sigma_f^2}{E_f} \int_0^{\ell/2} \frac{r_f^2}{4R^2} \frac{\left[\cosh \beta \left(\ell/2 - x\right) - 1 \right]^2}{\cosh^2 \beta \ell/2} dx$$

$$= \frac{6\pi r_f^2 \sigma_f^2}{E_f} \frac{r_f^2}{4R^2} \operatorname{sech}^2 \beta \ell/2 \left[3\ell/4 + \frac{\sinh \beta \ell}{4\beta} - \frac{2 \sinh \beta \ell/2}{\beta} \right] \quad \text{(viii)}$$

5.2.4.6. Energy released

Energy released $= E_c - E_{bf} - E_m$

$$= \sigma_c \varepsilon \pi R^2 \ell - \pi r_f^2 \varepsilon^2 E_f \left[\ell/2 - 2/\beta \tanh \beta \ell/2 + \frac{\sinh \beta \ell}{2\beta} \operatorname{sech}^2 \frac{\beta \ell}{2} \right]$$

$$= \tfrac{1}{2} \varepsilon^2 E_f \pi r_f^2 \ell + \tfrac{1}{2} \varepsilon^2 E_m \pi (R^2 - r_f^2) \ell - \pi r_f^2 \varepsilon^2 E_f \left[\ell/2 - \frac{1}{\beta} \tanh \frac{\beta \ell}{2} \right]$$

But $\beta = \frac{6}{\ell} \tanh \frac{\beta \ell}{2} \doteq 1$

$$\therefore \text{Energy released} = \pi \varepsilon^2 \ell r_f^2 \left[\tfrac{1}{2} E_f - \frac{E_f}{3} + \tfrac{1}{2} E_m \frac{R^2}{r_f^2} - \tfrac{1}{2} E_m \right]$$

$$= \pi \varepsilon^2 \ell r_f^2 \left[\frac{E_f}{6} + \tfrac{1}{2} E_m \frac{R^2 - r_f^2}{r_f^2} \right] \quad \ldots\ldots \text{(ix)}$$

5.2.4.7. Rate of release of energy

Normally $E_f > 10\, E_m$ so the first term predominates.

Hence in the Griffith - Irwin sense, for extension of the crack by area πR^2 the rate of release of energy

$$G_c = \frac{\delta E}{\delta A} = \frac{r_f^2}{R^2} \varepsilon^2 \ell \left(\frac{E_f}{6} + \tfrac{1}{2} E_m \frac{R^2 - r_f^2}{r_f^2} \right) \quad \ldots\ldots \text{(x)}$$

Note that this is more than $1/3$ of the originally stored energy.

5.2.4.8. Dissipation of released energy

The energy released in equation ix is used

(a) to increase the strain in adjacent fibres

(b) to supply surface energy for the new surfaces created

(c) to supply heat and acoustic energy and possibly energy for molecular deformation processes such as orientation.

The amounts are:

$$E_{af} = \frac{3\pi}{2}\frac{r_f^4}{R^2} E_f \operatorname{sech}^2 \frac{\beta \ell}{2} \left[\frac{3\ell}{4} + \frac{\sinh \beta \ell}{4\beta} - \frac{2 \sinh \beta \ell/2}{\beta}\right]$$

$$= \frac{7\pi}{80}\frac{r_f^4}{R^2} \varepsilon^2 E_f \ell$$

Surface energy for fibres $= 2 \gamma_f \pi r_f^2$

Surface energy for resin $= 2 \gamma_m \pi (R^2 - r_f^2)$

Dissipated energy $= E_d$

($\gamma_f \doteq 560$ ergs/cm^2 for glass. $\gamma_m \doteq 2 \times 10^4$ to 2×10^5 ergs/cm^2 for epoxy resin). Thus the energy equation becomes Energy released - Energy absorbed, i.e.

$$\pi \varepsilon^2 \ell r_f^2 \left[\frac{E_f}{6} + \tfrac{1}{2} E_m \frac{R^2 - r_f^2}{r_f^2}\right]$$

$$- \left[\frac{7\pi}{80}\frac{r_f^4}{R^2} \varepsilon^2 E_f \ell + 2\gamma_f \pi r_f^2 + 2\gamma_m \pi (R^2 - r_f^2) + Ed\right]$$

Dividing by $\pi R^2 \ell$ gives the energy per unit volume of the transfer zone:

$$\varepsilon^2 \frac{r_f^2}{R^2} \left[\frac{E_f}{6} + \tfrac{1}{2} E_m \left(\frac{R^2 - r_f^2}{r_f^2}\right)\right] - \left[\frac{7}{80}\left(\frac{r_f}{R}\right)^4 \varepsilon^2 E_f + \frac{2\gamma_f (r_f/R)^2}{\ell} + \frac{2\gamma_m}{\ell}\left(1 - \left(\frac{r_f^2}{R}\right)\right) + \frac{E_d}{\pi R^2 \ell}\right]$$

5.2.5. Criterion for fracture of neighbouring fibre

It is now possible to decide whether this difference is sufficient to break a neighbouring fibre.

For the six nearest neighbours of the broken fibre the probability that under a strain ε five will remain unbroken and the sixth will break when a strain increment $d\varepsilon$ is applied is:

$$6\left[1 - F(y)\right]^5 f(y)\, dy$$

where $y = \frac{\varepsilon - \bar{\varepsilon}}{\sigma}$, $F(y)$ the cumulative distribution function, $f(y) = \frac{dF}{dy}$ and σ the standard deviation.

Hence the expectation of another broken fibre in this set of six will be

$$36\left[1 - F(y)\right]^5 f(y)\, dy$$

and equating this to unity we find the condition that

$$dy = \frac{1}{36\,[1 - F(y)]^5\, f(y)} \qquad \ldots\ldots \text{(xi)}$$

for one of the six to break.

Example Now $dy = \frac{d\varepsilon}{\sigma} \doteqdot \frac{\varepsilon}{6\sigma}$

Hence $6\left[1 - F\left(\frac{\varepsilon - \bar{\varepsilon}}{\sigma}\right)\right]^5 f\left(\frac{\varepsilon - \bar{\varepsilon}}{\sigma}\right)\frac{\varepsilon}{\sigma} = 1$ (xii)

Table 9 gives calculated values of $6[1-F(y)]^5 f(y)$ for values of y from $-\infty$ to + 1.

An examination of the values shows that the maximum is at about $y = -1$ and is 0·611.

Hence $dy \doteqdot \frac{1}{6\times 0\cdot 611} = 0\cdot 273$

at $y = -1$ $\varepsilon = \sigma y + \bar{\varepsilon} = \bar{\varepsilon} - \sigma$

and $d\varepsilon \doteqdot \frac{\varepsilon}{6} = \sigma \times 0\cdot 273$

or $\varepsilon = 1\cdot 638\ \sigma$

i.e. $\bar{\varepsilon} = 2\cdot 638\ \sigma$

Hence if the coefficient of variation is less than 38% and the fibre is strained to within one standard deviation of the mean, catastrophic failure may occur.

If $y = -2$, $\bar{\varepsilon} = 5\cdot 47\ \sigma$ for catastrophic failure.

That is, if the coefficient of variation is lower than 18·3% the strain must not exceed two standard deviations from the mean.

5.2.6. Condition for crack propagation

The condition $dy = \frac{1}{36\,[1-F(y)]^5\, f(y)}$ for failure of one of the six adjacent fibres implies a value of the incremental energy which can then be used as a criterion.

In a system with strain energy $\frac{1}{2} E\varepsilon^2$ per unit volume an increase of strain to $\varepsilon + d\varepsilon$ means an increase in strain energy density by $E\varepsilon d\varepsilon$. Hence, if y is such as to satisfy

the equation xi above then, since $y = \frac{\varepsilon-\bar{\varepsilon}}{\sigma}$ we have the condition for propagation of a crack that the energy released on breakage of one fibre shall exceed the incremental strain energy derived from the term $E_f \varepsilon d\varepsilon$ at some point on a fibre. At this stage we shall assume that it is not the total energy in the transfer zone but the energy density at a point on an adjacent fibre that is the critical factor. Hence our criterion for failure is

$$\text{Energy released} - \text{Energy absorbed} > E_f \varepsilon \delta\varepsilon \qquad \ldots\ldots \quad \text{(xiii)}$$

where ε and $d\varepsilon$ are related by the statistical condition above, that is,

$$\delta\varepsilon = \frac{\sigma}{36\left[1-F\left(\frac{\varepsilon-\bar{\varepsilon}}{\sigma}\right)\right]^5 f\left(\frac{\varepsilon-\bar{\varepsilon}}{\sigma}\right)}$$

5.2.7. Time dependence of modes of failure

5.2.7.1. Elementary example

In a bundle of N_o fibres the expectation of failure up to and including y is $N = N_o F(y)$ where $y = \frac{\varepsilon-\bar{\varepsilon}}{\sigma}$

Now $\frac{dN}{dt} = N_o f(y) \frac{1}{\sigma} \frac{d\varepsilon}{dt}$

$= N_o f(y) \frac{\nu}{\sigma}$ if $\frac{d\varepsilon}{dt} = \nu$

$\therefore \quad dN = N_o f(y) \frac{\nu dt}{\sigma}$

Hence the average time for one fibre to break will be

$$dt = \frac{\sigma}{N_o f(y) \nu} \cdot 1 \qquad \ldots\ldots \quad \text{(xiv)}$$

If this time exceeds the retardation time T of the resin the stress in the resin will have time to relax, reducing the strain energy available. If it is shorter than T then strain cannot relax before a fibre is due to break, and strain magnification will be present.

For the six nearest neighbours

$$\Delta N = 36\left[1 - F(y)\right]^5 f(y) \quad \Delta y$$

and $\frac{\Delta N}{\Delta t} = 36\left[1 - F(y)\right]^5 f(y) \quad \frac{\nu}{\sigma}$

Hence for the breakage of one fibre of the six, a time Δt is required

$$\Delta t = \frac{\sigma}{36\left[1 - F(y)\right]^5 f(y)\ \nu} \qquad \ldots\ldots \text{(xv)}$$

In this time the energy density will change as the modulus of the resin changes from its unrelaxed to a more relaxed state according to the relation (for a simple spring dashpot model):

$$E(\Delta t) = E_R + (Eu - E_R)e^{-\frac{\Delta t}{T}}$$

Hence the inequality (xiii) becomes

$$\varepsilon^2 \frac{r_f^2}{R2}\left[\frac{E_f}{6} + \frac{1}{2}\left(\frac{R^2 - r_f^2}{r_f^2}\right)\left\{E_R + \left(E_u - E_R\right)\exp\left(\frac{-\sigma}{36\left[1-F(y)\right]^5 f(y)\,\nu\,T}\right)\right\}\right]$$

$$-\left[\frac{7}{80}\left(\frac{r_f}{R}\right)^4 \varepsilon^2 E_f + \frac{2\gamma_f}{\ell}\left(\frac{r_f}{R}\right)^2 + \frac{2\gamma_m}{\ell}\left(1 - \left(\frac{r_f}{R}\right)^2\right) + \frac{E_d}{\pi R^2 \ell}\right]$$

$$> \frac{E_f\ \varepsilon\ \sigma}{36\left[1-F\left(\frac{\varepsilon-\bar{\varepsilon}}{\sigma}\right)\right]^5 f\left(\frac{\varepsilon-\bar{\varepsilon}}{\sigma}\right)} \qquad \ldots\ldots \text{(xvi)}$$

This inequality gives the strain for brittle failure in terms of parameters of the composite.

Clearly brittle failure is more likely when E_f is large, when T is small, or when ν or T are large. The equation also takes into account the proximity of ε to $\bar{\varepsilon}$ the mean breaking strain of the fibres through the presence of f(y) in the denominator of the right hand side. The retardation time T is of course temperature dependent, low temperatures giving long retardation times.

For maximum toughness a medium to low proportion of fibres, preferably of very variable strength, and of large diameter (since this increase $\ell/2$ the transfer length) is required. Supporting evidence for this comes again from work on fibre reinforced metals by Cooper and Kelly (42).

The importance of the rate of testing is shown by McAbee and Chmura (40) who tested fibreglass laminates at varying speeds, finding higher strength and modulus at the higher rates of strain.

The author (50) has shown that the mode of failure of a longitudinally reinforced resin sample when tested in tension depends critically upon the rate of testing; slower rates led to a more fibrous type of fracture while high speeds gave a brittle type.

ane effect of fibres upon each other during fracture has been seen to be the same whether in a fibre reinforced material or, by considering molecular chains as "fibres", in a resin. The same effect is found in the tearing of textiles in work published by Taylor [43], O'Brien and Weiner [44], Spencer-Smith [45] and Kilby [46]. The general conclusion is that when interfibre effects are small (low twist, low interfibre friction) the tear strength is high while if the fibres are highly twisted or woven in such a way that friction is high, or coated with crease resistant or fire resistant finishes, then the tear resistance will be low. This latter case corresponds to the fibre reinforcement condition of a short transfer length.

It is not yet possible to answer qualitatively the question "Are strength and toughness incompatible?" To do this a more careful study of the energy changes in fracture of a composite is needed, taking into account all energy absorbing mechanisms such as the one proposed by Cook and Gordan [47].

5.3. Predictions from the theory

Using equation (xvi) as a criterion of brittle fracture, calculations were made, using a computer, for typical conditions for a glass fibre epoxy resin system. The input data were:

E_f	= $7{\cdot}3 \times 10^{10}$	N/m^2
G_R (resin)	= $2{\cdot}1 \times 10^{6}$	N/m^2
G_U (resin)	= $1{\cdot}05 \times 10^{9}$	N/m^2
γ_f (glass)	= 0·56	J/m^2
γ_m (resin)	= 2 × 10	J/m^2

Concentration of fibres:	10% to 70% by volume
Strain rates:	10^{-5}, 10^{-3}, 10^{-1}
Retardation times:	1000, 1, 1/1000s
Mean fibre breaking strains $\bar{\varepsilon}$:	0·0001, 0·01, 0·1
Standard deviations:	$0{\cdot}1\bar{\varepsilon}$, $0{\cdot}5\bar{\varepsilon}$

The strain ε was then varied from zero to $\bar{\varepsilon}$ in steps of $0{\cdot}1\ \bar{\varepsilon}$ and by linear interpolation the value of ε for catastrophic failure was then found.

The results are given graphically in figures 31 to 34. Examination of these figures indicates the following conclusions:

(a) Catastrophic failure should never occur when $T = 0{\cdot}5\ \bar{\varepsilon}$

(b) Catastrophic failure should never occur when $\bar{\varepsilon} = 0{\cdot}001$ (0·1% strain)

(c) For $\bar{\varepsilon} = 0{\cdot}01$ (1% strain) (Fig.31), the strain at which catastrophic failure will occur falls as the concentration of fibres is increased from about $0{\cdot}9\ \bar{\varepsilon}$ at 20% concentration to $0{\cdot}81\varepsilon$ at 70%. Below 20% concentration catastrophic failure should not occur.

The curve for short time-constant (resin in rubbery state) lies below the curve for longer time-constants. Thus if the resin is in the glassy state or a rapid strain rate is employed this results in a higher breaking strain than occurs in the rubbery state.

If the size of the reinforcing fibre is 10 micron (Fig.32) instead of 100 micron theory indicates that catastrophic failure should not occur except for the rubbery state ($T = 1/1000$) and for the slowest strain rate in the intermediate state ($T = 1$). Thus on this theory, for medium strength fibres ($\varepsilon = 0{\cdot}01$) the smaller fibres result in a tougher material.

(d) For $\varepsilon = 0{\cdot}1$ (10% strain) (Fig.33), the fibres are of maximum strength and the pattern of behaviour is somewhat different from that found for low strength fibres. The same trend to lower breaking strains at higher fibre concentrations is, however, found but the curves for the rubbery state now lie above those for the glassy state and the curve for the lowest strain rate lies above those for the higher rates, for any one choice of T. Thus a material reinforced with very strong, uniform fibres ($\sigma = 0{\cdot}1\bar{\varepsilon}$) will be tougher at low rates of strain and in the rubbery state (νT low) than at high rates of strain or in the glassy state (ν T high). There is little change with the radius of the reinforcing fibres, the curves for $r_f = 10\mu$ (Fig.34) being very similar to those for $r_f = 100$.

5.4. Discussion

The foregoing theory is an attempt to introduce quantitative relationships into the subject of the fracture of fibre reinforced resins and to take into account rate effects.

It has already been noted by Kelly [38] that too high a concentration of fibres in a metal matrix gives a brittle composite and the same is true in a resin reinforced by fibres, (Wadsworth and Spilling [51]. The analogy with the effect of cross linking on the strength of rubbers, analysed for example by Bueche [39], is close and it is suggested that this is because the theory required is the same in the two cases.

Experimental work shows that a highly cross linked resin is more brittle than one in which a proportion of possible cross links have not been formed. Thus Lewis and Ramsey's [26] results and the findings of Van den Boogaart [41] together with the work of Burhans [28] suggest that maximum toughening in a pure resin occurs when it is undercured. Can these results be explained by considering a polymer network as though it were a molecular scale fibre-reinforced material? This is effectively the basis of Bueche's treatment of a cross linked network and it is obviously qualitatively satisfactory. It is proposed to add to Bueche's theory

(a) the concept of transfer length

(b) the consideration that chains may have very variable breaking extensions

(c) the retardation time of the resin.

From the latter concepts it is predicted, using calculated results from the reinforcement theory, that if the breaking extensions of the chains are very uniform brittle failure is to be expected (glassy state) whereas if they are variable it is expected that the failure of one chain will be accommodated by its neighbours in a reasonable time.

The time to be considered is that for the relaxation of stress in the neighbourhood of a broken chain. The relevant relaxation time will therefore be that for a small chain segment, that is the γ relaxation at low temperatures. Neilsor. [31] states that at temperatures well below T_g two rigid polymers can differ greatly in impact strength. For example, cellulose nitrate and polycarbonates show much higher impact strengths than polystyrene or PMMA: Neilsen holds that this is due to the secondary transitions in the former polymers (see also Bobalek and Evans [48]).

In epoxy resins there are two well defined relaxation regions. The α-relaxation or glass rubber transition, depending upon the hardener used and the resin system, lies above 100°C and is the main transition region. The γ or low temperature transition lies below -50°C and is associated with the opening of the epoxy ring to form a bond with the hardener.

The curing of an epoxy increases the intensity of this relaxation and shifts it (in an amine cured resin) from about -75°C to -50°C. The use of a flexible hardener (e.g. dodecynyl succinic anhydride) moves the γ peak to -90°C and introduces a subsidiary δ peak at -160°C (Speake [49]). The same shift of the γ peak to lower temperatures is found by the incorporation of Araldite X83/219 (diglycidyl ether of polypropylene glycol) into the network structure and in this case also a δ peak starts to appear at about -140°C. Chemical undercure has also been shown to move the γ peak to lower temperatures. Undercured materials are tougher than resins made without the flexible groups, the impact strength being increased by a factor of about 2.

We may be able to explain the increased toughness (or resistance to catastrophic failure) of these resins by using the fibre reinforcement model and taking the relaxation time relevant to the γ relaxation. This is a low energy transition and moves about 6 to 10°C per decade of frequency. The results quoted were obtained at 1 Hertz so that at room temperature the -50°C relaxation should appear at about 1 megahertz. Thus the relaxation time at room temperature can be taken as 10^{-6} second. For the lower temperature relaxations found when flexible groups are used in either resin or hardener the relaxation time may well be 10^{-9} second.

Thus at reasonable strain rates the product νT in equation (xvi) will be very small and the material will behave in a rubbery fashion. That is, the breakage of one chain will be rapidly accommodated by the neighbouring chains and the transfer zone will be large, the crack blunted. At higher rates of strain νT may approach glassy values if T is only 10^{-6} but is unlikely to if it is 10^{-9}. Thus under impact conditions the material is likely to be tougher when the γ peak lies below 50°C.

It may be possible to be more quantitative in the use of the fibre reinforcement analogue and to design a resin for toughness and strength possibly by choosing copolymer blends to give the right balance between load bearing chains and energy absorbing ones.

One may expect the pure resin, pure hardener system to be virtually useless because of brittleness but that a distribution of molecular weights and a mixture of different hardeners would give optimum properties. Much remains to be done, however, before such molecular engineering is possible.

6. CONCLUSIONS

6.1. Modulus in the glassy region

Within the glassy region the agreement between predicted and measured values of the shear modulus is good. Since predicted values for specimens cut at various angles to the fibres axis involve all five predicted elastic constants it can be inferred that all five are reasonably accurate. The experimental values all tend to lie above the predicted ones, however, in agreement with the comment by Chamis and Sendeckyj[8].

6.2. Modulus in the rubbery region

In the rubbery region, good agreement is not obtained. It is difficult to account for this discrepancy other than by assuming that it is the basic assumptions of the theories which are in error. Thus it is by no means certain that resin in the interstices between fibres has the same elastic properties that it has in the bulk. There are also unknown compressive stresses involved which may play a part. However, it is likely that the largest error consists in using a homogeneous anisotropic model for a heterogeneous material and it is possible that a much larger specimen would have approximated better to the homogeneous ideal.

6.3. Tan δ

Turning to the loss factor the epperiments show clearly that for the system used it is perfectly valid to substitute complex quantities for the elastic moduli in explicit formulæ such as those of Whitney-Riley, Hashin or Van Fo Fy and Savin, and that the predicted tan δ curve corresponds closely to that observed provided that chemical interaction of surface active agents with the resin and secondary sources of energy absorption are taken into account.

A comparison of our results with predictions based on other theories now available may make it possible to state which explicit formulæ are the best to use for predicting the complex moduli of a fibre reinforced system.

7. REFERENCES

1. Z. Hasin and B. Rosen (1964) J. Appl. Mech., Trans. ASME 31, 223
2. R. Hill (1964) J. Mech. Phys. Solids, 12, 199
3. J. M. Whitney and M.B. Riley (1966) AIAA Journal, 4, 1537
4. G.A. Van Fo Fy and G.N. Savin (1965), Mekh. polim. 1, 151
5. M.D. Heaton, 1968 Brit. J. Appl. Phys. (J.Phys. D) (2) 1, 1039
6. G. Pickett, in Fundamental aspects of f.r. plastic composites (Inter-science 1968)
7. C. H. Chen and S. Cheng (1967) J. Composite Materials 1, 30
8. C.C. Chamis and G.P. Sendeckyj (1968) J. Composite Materials 2, 332
9. R.F.S. Hearmon (1961) Applied Anisotropic Elasticity (O.U.P.)
10. W. Voigt (1928) Lehrbuch der Kristallphysik (Teubner)
11. M.A. Biot (1954) J. Appl. Phys. 25, 1385
12. T.G. Rogers and A.C. Pipkin (1963) ZAMP 14, 334
13. Z. Hashin (1965) J. Mech Phys. Solids 13, 119
14. T.G. Rogers - private communication
15. L.E. Neilson, Mechanical properties of polymers

16. Kono (1961) J. Phys. Soc. Japan 16, 1580

17. S. Sterman and J.G. Marsden (1963) Proc. 18th Ann. Conf. S.P.I. Section 1D

18. J.M. O'Reilly (1962) J. Polymer Sci. 57, 429

19. L.C.E. Struik (1967) Rheol. Acta 6 (2), 119

20. L. Broutman and G. Krock, Modern Composite Materials (Addison - Wesley 1968)

21. E. Orowan (1949) Rep. Progr. Phys. 12, 185

22. G.R. Irwin (1948) Fracturing of Metals, p.147. Am. Soc. Metals, Cleveland, Ohio

23. R.S. Rivlin and A.G. Thomas (1953) J. Polymer Sci. 10, 291

24. F.J. McGarry and G.C. Selfridge (1963) M.I.T. Research Report R63-46

25. L.J. Broutman (1963) M.I.T. Research Report R63-35

26. A.F. Lewis and W.B. Ramsey (1966) Adhesives Age 9 (2), 20

27. S. Mostovoy and E.J. Ripling (1966) J. Appl. Polymer Sci. 10, 1351

28. A.S. Burhans et al (1966) SPI/21 R.P. Conf. Section 14c

29. A. Kelly (1966) Strong Solids (Clarendon Press, Oxford)

30. H.L. Cox (1952) Brit. J. Appl. Phys. 3, 72

31. L.E. Neilsen, Mechanical Properties of Polymers

32. A.E. Lever and J. Rhys (1962) The Properties and Testing of Plastic Materials (Temple Press)

33. L. Holliday Composite Materials

34. G. Hulse (1965) Physics of Plastics (Iliffe)

35. G.R. Irwin (1958) "Fracture" in Handbuch der Physik (Springer-Verlag)

36. P.I. Vincent (1966) Physical Basis of Yield and Fracture (Institute of Physics, London)

37. E.G. Bobalek and R.M. Evans SPI/15 R.P. Conference 12-E

38. A. Kelly (1964) Proc. Roy. Soc. A 282, 63

39. F. Bueche (1957) J. Polymer Sci. 24, 189

40. E. McAbee and M. Chmura (1965) Applied Polymer Symposia 1, 85-98

41. A. Van den Boogaart (1966) Physical Basis of Yield and Fracture (Institute of Physics, London)

42. G.A. Cooper and A. Kelly (1967) J. Mech. Phys. Solids 15, 279

43. A.W. Taylor (1959) J. Text. Inst. 50, T161

44. W.E. O'Brien and L.I. Weiner (1954) Text. Res. J. 24, 241

45. J.L. Spencer-Smith (1947) J. Text. Inst. 38, 257

46. W.F. Kilby (1964) J. Text. Inst. 55, T589

47. J. Cook and J. E. Gordon (1964) Proc. Roy. Soc. A282, 508

48. E.G. Bobalek and R.M. Evans (1961) S.P.E. Trans. 1 (2), 93

49. J.H. Speake - private communication

50. R.G.C. Arridge (1969) Nature 225, 941

51. N.J. Wadsworth and I. Spilling (1968) Brit. J. Appl. Phys. (J. Phys. D.), Ser. 2, Vol.1, 1049

TABLE 1

DETAILS OF CASTS

CAST No.	DISTANCE BETWEEN FIBRES, mm	NOMINAL CONTRACTION, v/v	FINISH APPLIED	CURE
13	0·50	3%	Yes	24 hrs 130°C
* 15	0·50	3%	No	16 hrs 100°C +24 hrs 140°C
16	0·25	12%	Yes	16 hrs 100°C +24 hrs 130°C
17	0·25	12%	Yes	17 hrs 105°C +24 hrs 130°C
18	0·25	12%	Yes	24 hrs 110°C +24 hrs 130°C
20	0·12	40%	Yes	20 hrs 110°C 24 hrs 130°C
29	0·13	40%	No	17½ hrs 98°C + 9 hrs 115°C +24 hrs 145°C
30	Unknown	Maximum	Yes	16 hrs 110°C +26 hrs 155°C
33	Unknown	Maximum	No	17 hrs 120°C +26 hrs 157°C
34	Unknown	Maximum	Yes	17 hrs 108°C +24 hrs 158°C
35	-	0	No	19 hrs 110°C +27 hrs 158°C
37	-	0	No	19 hrs 110°C +27 hrs 158°C
42	Unknown	Maximum	No	22 hrs 110°C +25 hrs 157°C
43	Unknown	Maximum	No	22 hrs 110°C +25 hrs 157°C
45	Control for 42 and 43			

* Cast 15 was not cast under vacuum nor was vacuum treatment used after casting. The remainder were either poured under vacuum or underwent a series of cycles of about 2 minutes each to remove air bubbles.

TABLE 2

COMPARISON BETWEEN CONTROL SAMPLES

TEMPERATURE °C	SHEAR MODULUS, (GN/m^2)				
	CAST 13	CAST 15	CAST 16	CAST 18	CAST 20
20	0·93		0·98	1·00	0·90
25	0·85	0·87	0·90	0·95	0·95
30	0·68	0·83	0·80	0·84	0·79
35	0·55	0·72	0·70	0·64	0·65
40	0·40	0·56	0·55	0·44	0·50
80	0·00195	0·00250	0·00260	0·00250	0·00210
85	0·00200	0·00240	0·00235	0·00240	0·00210
90	0·00205	0·00250	0·00220	0·00245	0·00215
95	0·00220	0·00255	0·00220	0·00250	0·00215
100	0·00235	0·00260	0·00225	0·00250	0·00220
	Damping factor, tan δ				
25	0·058	0·033	0·028	0·032	0·030
30	0·082	0·042	0·042	0·038	0·036
35	0·125	0·066	0·064	0·050	0·048
40	0·220	0·120	0·100	0·080	0·088
80		0·122	0·430	0·190	0·200
85	0·150	0·102	0·160	0·090	0·105
90	0·090	0·060	0·070	0·046	0·060
95	0·052	0·030	0·036	0·025	0·030
100	0·033	0·014	0·021	0·013	0·015

TABLE 3

MEASURED VALUES OF FIBRE CONCENTRATION

SPECIMEN CAST No.	METHOD USED	SPECIMEN ORIENTATION				
		0°	30°	45°	60°	90°
		% FIBRE v/v				
13	Density	3·45	3·15	3·05	3·05	3·05
	Ash	3·20	3·02	2·99	2·93	3·02
	Mean	3·3	3·1	3·0	3·0	3·0
15	Density	2·45	2·65	2·55	2·55	2·55
	Ash	2·75	2·58	2·58	2·59	2·55
	Mean	2·6	2·6	2·6	2·6	2·5
16	Density	7·45	8·7	7·04	8·70	10·31
	Ash	7·43	8·34	6·69	8·52	9·87
	Mean	7·4	8·5	7·0	8·6	10·1
18	Density	12·68	14·42	15·34	1 ·42	12·68
	Ash	12·61	14·29	15·02	14·32	12·67
	Mean	12·7	14·4	15·2	14·5	12·7
20	Density	38·37	38·67	41 43	37·76	34·59
	Ash	-	38·79	40·16	37·84	34·82
	Mean	38·4	38·7	41·2	37·8	34·7
29	Density	32·93	31·50	31·50	31·20	30·28
	Ash	32·80	31·24	31·59	31·41	31·08
	Mean	32·9	31·4	31·5	31·3	30·7
30	Density	41·27	36·95	36·49	37·26	41·34
	Ash	40·95	37·41	-	37·56	44·98
	Mean	41·1	37·2	36·5	37·4	43·2
33	Density	72·76	-	-	-	-
	Ash	76·94	-	-	-	-
	Mean	73·8	-	-	-	-
34	Density	47·11	-	-	-	-
	Ash	48·06	-	-	-	-
	Mean	47·6	-	-	-	-
42	Density	56·43	-	-	-	-
	Ash	58·86	-	-	-	-
	Mean	57·6	-	-	-	-
43	Density	53·87	-	-	-	-
	Ash	53·80	-	-	-	-
	Mean	53·8	-	-	-	-

TABLE 3 (cont.)

	SPECIMEN		% FIBRE v/v
CAST No.	TEST LENGTH	METHOD USED	
17	55 mm	Density	9·90
	56 mm	Density	9·73
	40 mm	Density	11·63
	40 mm	Density	12·37

TABLE 4

EFFECT OF SPECIMEN LENGTH ON MEASURED AND CALCULATED SHEAR MODULUS

CAST No.	SPECIMEN TEST LENGTH	TEMP. ^{o}C	MEASURED MODULUS (GN/m^2)	CALCULATED MODULUS (GN/m^2)
17	55 mm	25 100 25	1·31 0·00421 1·27	1·11 0·00298 1·15
	56 mm	25 100 25	1·42 0·00422 1·39	1·11 0·00296 1·15
	40 mm	25 100 25	1·19 0·00415 0·96	1·15 0·00308 1·19
	40 mm	25 100 25	1·19 0·00407 0·99	1·17 0·00313 1·21
35 (Control)	40 mm	25 100 25	9·24 0·00244 9·56	- - -

TABLE 5

CALCULATED MODULUS AND TAN δ VALUES FOR S_{12} VARYING FROM ½ S_{21} TO 2 S_{21} (CAST 20)

TEMPERATURE °C	S_{12}/S_{21}	ANGLES BETWEEN FIBRES AND SPECIMEN AXES					
		30°		45°		60°	
		MODULUS (GN/m^2)	TAN δ	MODULUS (GN/m^2)	TAN δ	MODULUS (GN/m^2)	TAN δ
20	½	2·52	·0258	2·57	·0270	2·16	·0280
	1	2·50	·0256	2·53	·0268	2·12	·0280
	2	2·49	·0249	2·48	·0266	2·07	·0279
25	½	2·42	·0302	2·47	·0316	2·07	·0328
	1	2·40	·0299	2·43	·0314	2·03	·0328
	2	2·40	·0292	2·38	·0311	1·48	·0317
30	½	2·25	·0418	2·28	·0436	1·91	·0452
	1	2·24	·0414	2·25	·0434	1·87	·0451
	2	2·23	·0404	2·21	·0430	1·83	·0450
35	½	1·89	·0752	1·91	·0784	1·59	·0808
	1	1·89	·0745	1·88	·0781	1·56	·0807
	2	1·89	·0729	1·85	·0774	1·52	·0805
40	½	1·50	·135	1·50	·140	1·23	·144
	1	1·50	·134	1·48	·140	1·21	·144
	2	1·51	·131	1·46	·139	1·19	·144
45	½	1·08	·230	1·07	·238	0·875	·243
	1	1·08	·229	1·06	·237	0·861	·242
	2	1·10	·225	1·04	·236	0·842	·242
50	½	0·704	·386	0·686	·396	0·556	·401
	1	0·706	·384	0·678	·395	0·547	·401
	2	0·722	·379	0·671	·394	0·536	·401

TABLE 6

EFFECT OF ASSUMING DIFFERENT VALUES FOR POISSON'S RATIO ON SHEAR MODULUS (G)

POISSON'S RATIO	TEST TEMP.	SHEAR MODULUS (GN/m^2)				
		ANGLE BETWEEN FIBRES AND SPECIMEN AXES				
		0^o	30^o	45^o	60^o	90^o
0·35	45°C	0·78	1·08	1·06	0·86	0·68
0·40		0·78	1·10	1·08	0·88	0·69
0·45		0·78	1·12	1·11	0·91	0·70
0·35	50°C	0·49	0·71	0·68	0·55	0·43
0·40		0·49	0·71	0·69	0·56	0·43
0·45		0·49	0·73	0·71	0·58	0·44

TABLE 7

TYPICAL IMPACT STRENGTHS OF VARIOUS MATERIALS

MATERIAL	IMPACT STRENGTH (Nm/mm WIDTH)	
	IZOD	CHARPY
Steel		1·6 to 6·4
Aluminium		1·1
Phenol formaldehyde (unfilled)	0·1 to 0·2	0·016 to 0·02
Phenol formaldehyde (fabric filled)	0·05 to 0·21	
Phenol formaldehyde (laminates)	0·54 to 2·7	0·05 to 0·2
Melamine		0·02
Melamine laminates		0·04 to 0·05
Polyester	0·01 to 0·02	
Polyester laminates	0·08 to 0·9	
Epoxy	0·01 to 0·05	
Epoxy laminates	0·4 to 0·8	
Polyethylene low density	0·86	
Polyethylene high density	0·03 to 0·2	
Polyvinyl chloride rigid	0·02 to 0·05	
Polyvinyl chloride polyblend	0·16 to 0·80	
Nylon 66	0·05	
Nylon (glass filled)	0·16 to 0·32	
Polystyrene	0·013 to 0·032	
Polystyrene (ABS)	0·05	
PMMA	0·02	0·02

TABLE 8

TYPICAL SURFACE ENERGIES OF VARIOUS MATERIALS

MATERIAL	CHARACTERISTIC SURFACE ENERGY G_o (10^{-4} J/mm^2)	
Steel, ship plate ductile	3500	k
Aluminium alloy	260 - 1050	k
Polymethyl methylacrylate (tension)	8·7	k
Polyesters	2·0	k
Vulcanized natural rubber	120	k
Glass lantern slide covers (moist)	0·07	k
Cellulose acetate	50	k
Polystyrene cleavage	4	l
Polymethyl methacrylate cleavage	1·2	l
Polyester cleavage	0·1	l
Epoxy cleavage	0·2 - 2·0	l
Hot-stretched polystyrene (parallel to stretch)	0·07	m
Epoxy (DER 332) and glass laminate	3	n
Impact resistant polystyrene ABS	50 - 140	n

Data from: k Irwin (Ref.35)
l McGarry and Selfridge (Ref.24)
m Broutman (Ref.25)
n McGarry and Selfridge (Ref.24)

TABLE 9

CALCULATED VALUES OF $6\,[1-F(y)]^5\,f(y)$

$y = \frac{\varepsilon - \bar{\varepsilon}}{\sigma}$	$6\,[1-F(y)]^5\,f(y)$
$-\infty$	0
- 5	$0{\cdot}9 \times 10^{-6}$
- 4	$0{\cdot}8 \times 10^{-3}$
- 3	$0{\cdot}264 \times 10^{-1}$
- 2	0·288
- 1·5	0·546
- 1	0·611
- 0·5	0·481
0	$0{\cdot}75 \times 10^{-1}$
1	$0{\cdot}243 \times 10^{-3}$

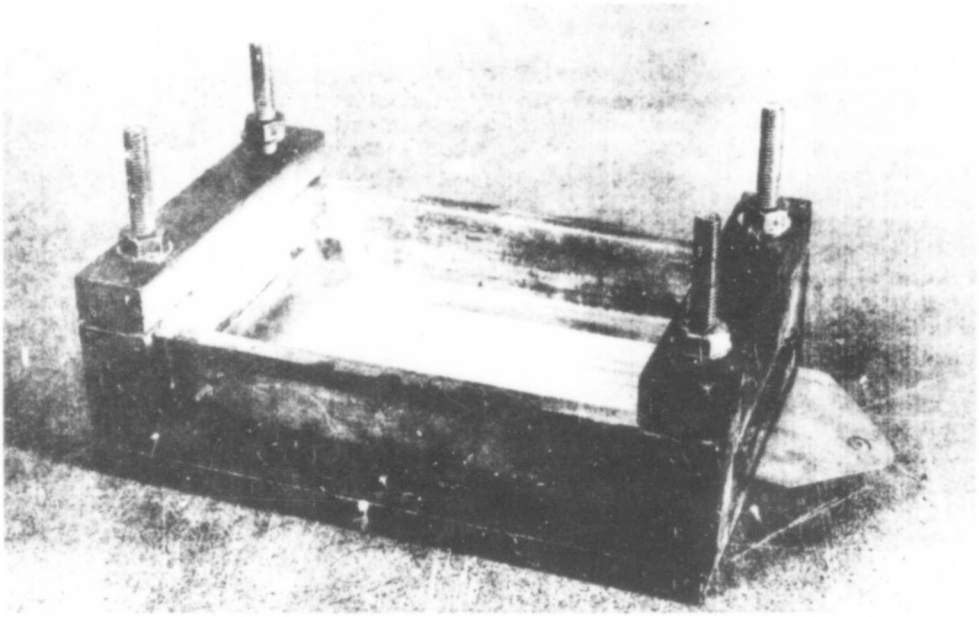

FIG. 1 MOULD FOR UNIDIRECTIONAL ARRAYS

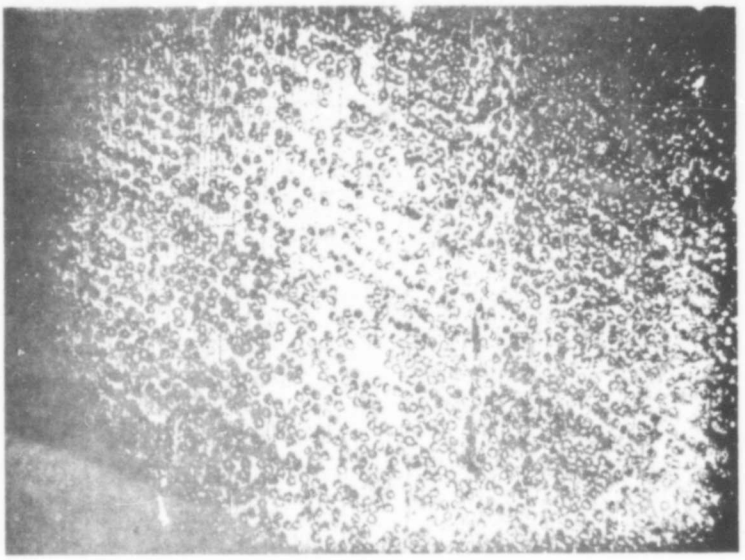

FIG. 2

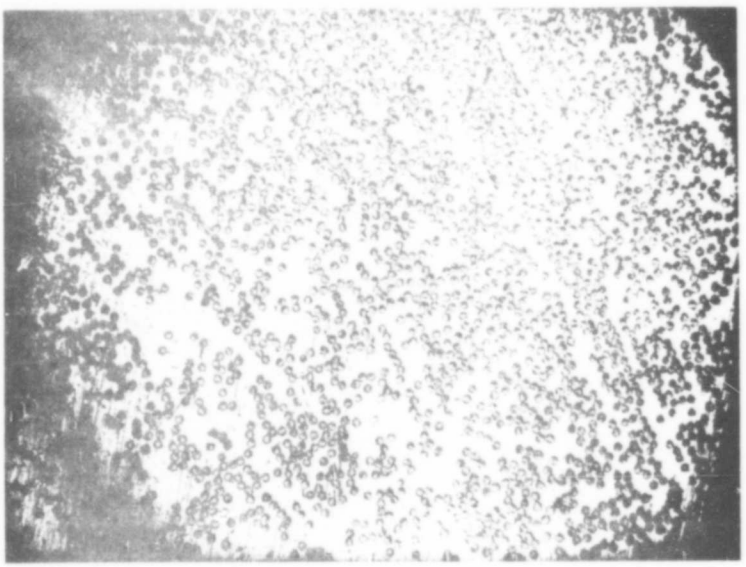

FIG. 3

FIG. 4

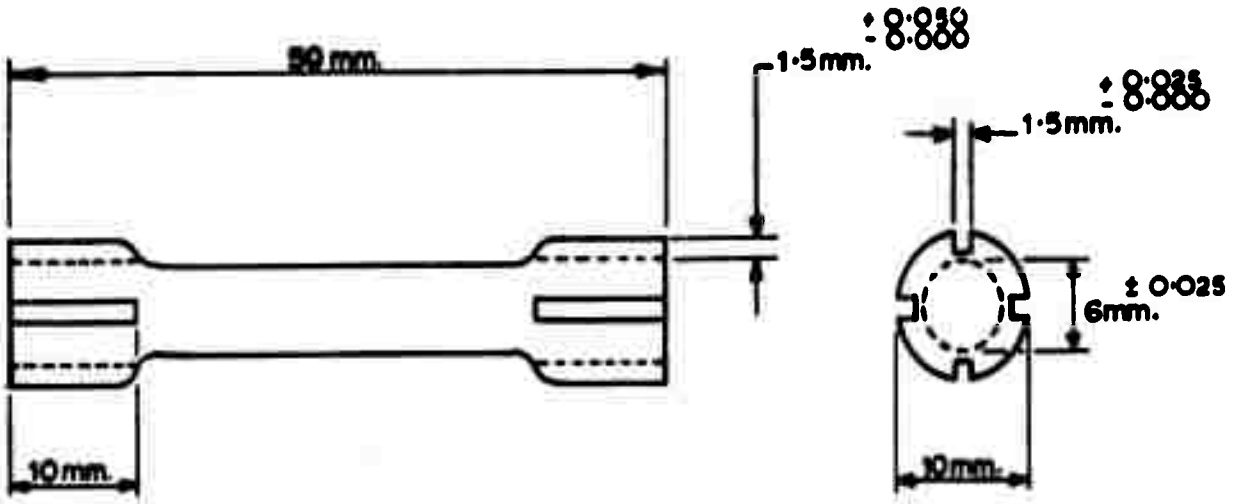

FIG. 5 SPECIMEN DETAILS

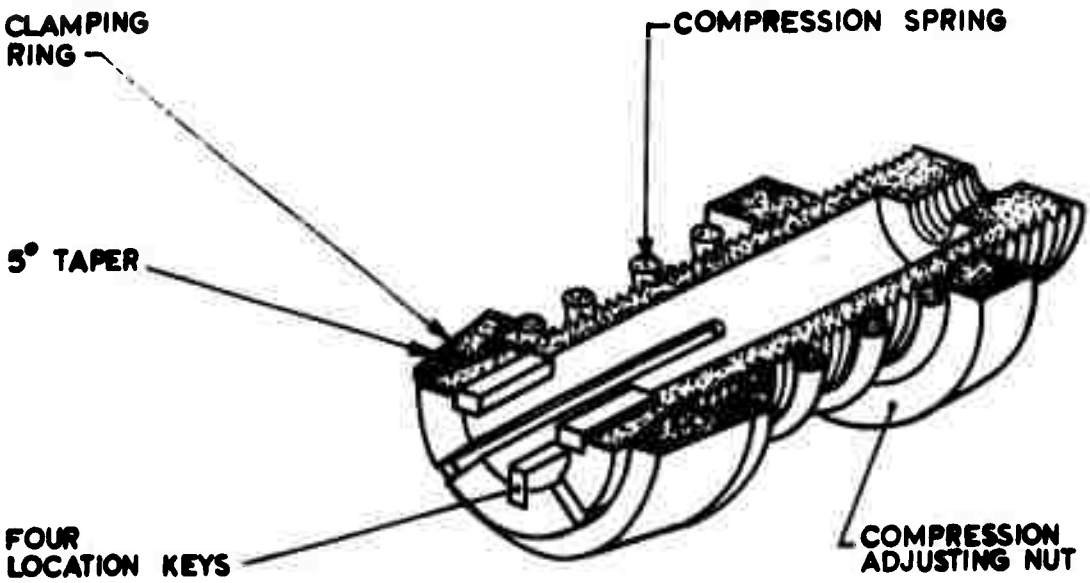

SECTIONAL VIEW

FIG. 6 SPECIMEN GRIPS

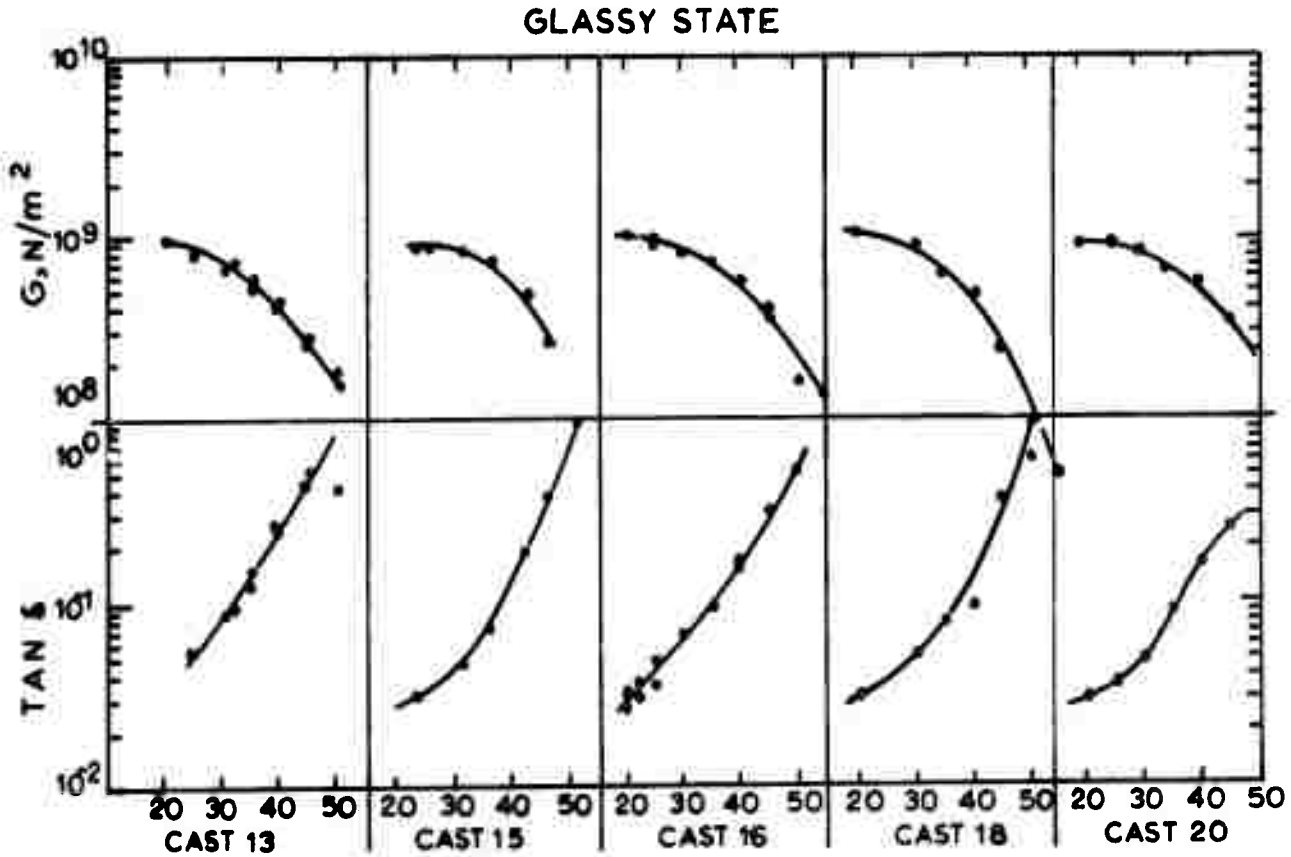
GLASSY STATE
G, N/m²
TAN δ
CAST 13
CAST 15
CAST 16
CAST 18
CAST 20

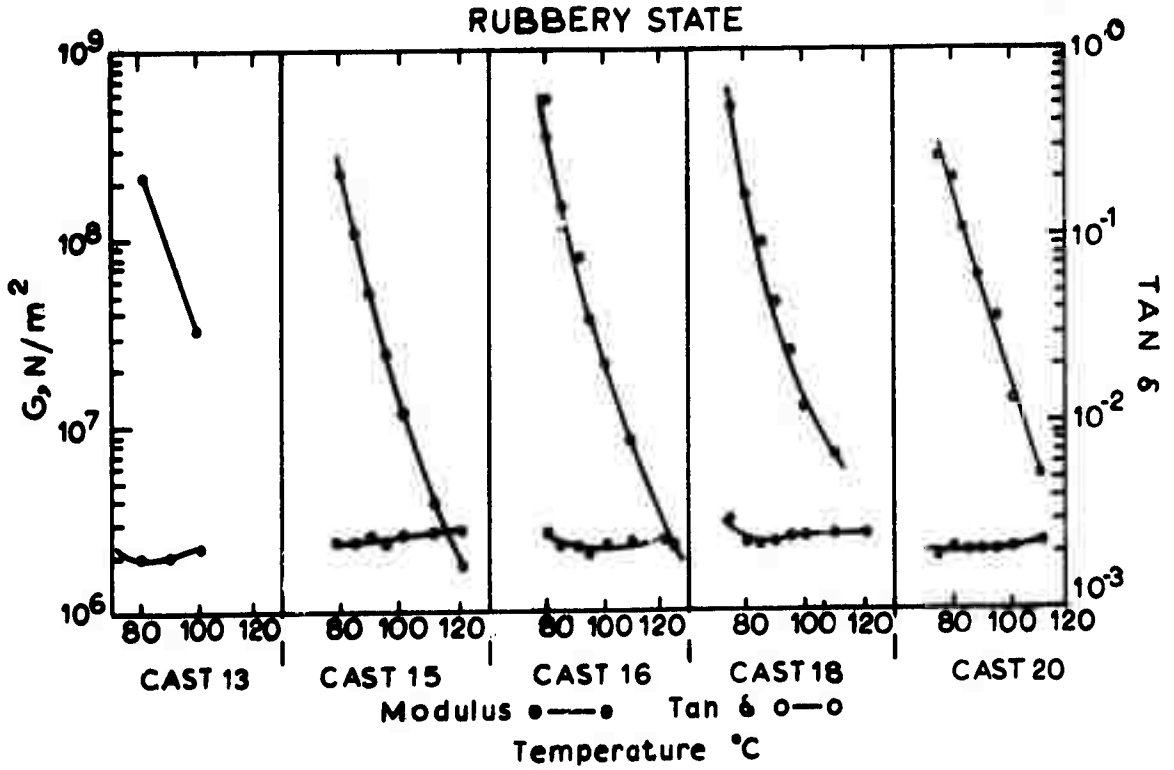
RUBBERY STATE
G, N/m²
TAN δ
CAST 13
CAST 15
CAST 16
CAST 18
CAST 20
Modulus •—•
Tan δ o—o
Temperature °C

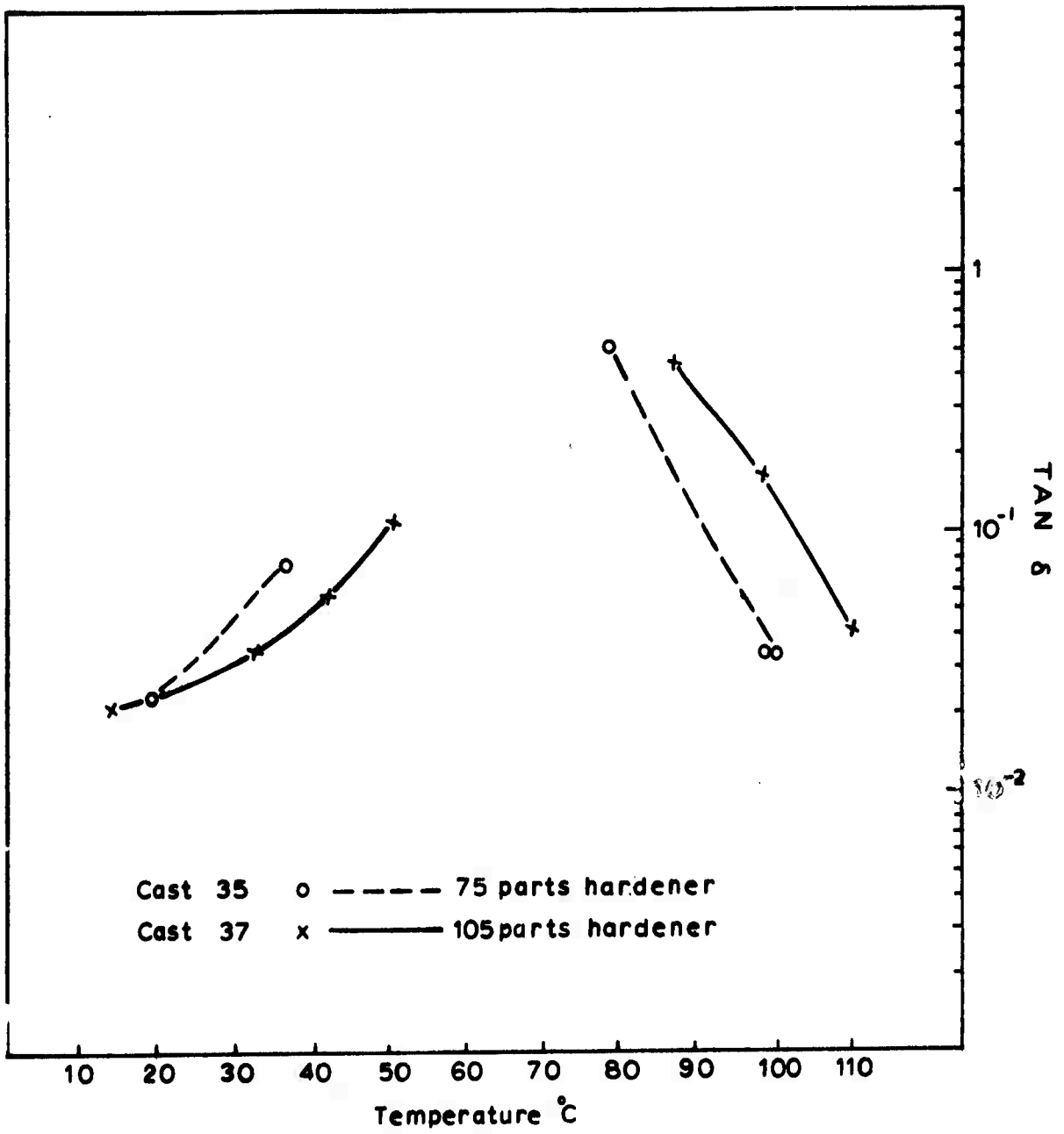

Fig 8. Effect of Increasing Hardener on Tan δ

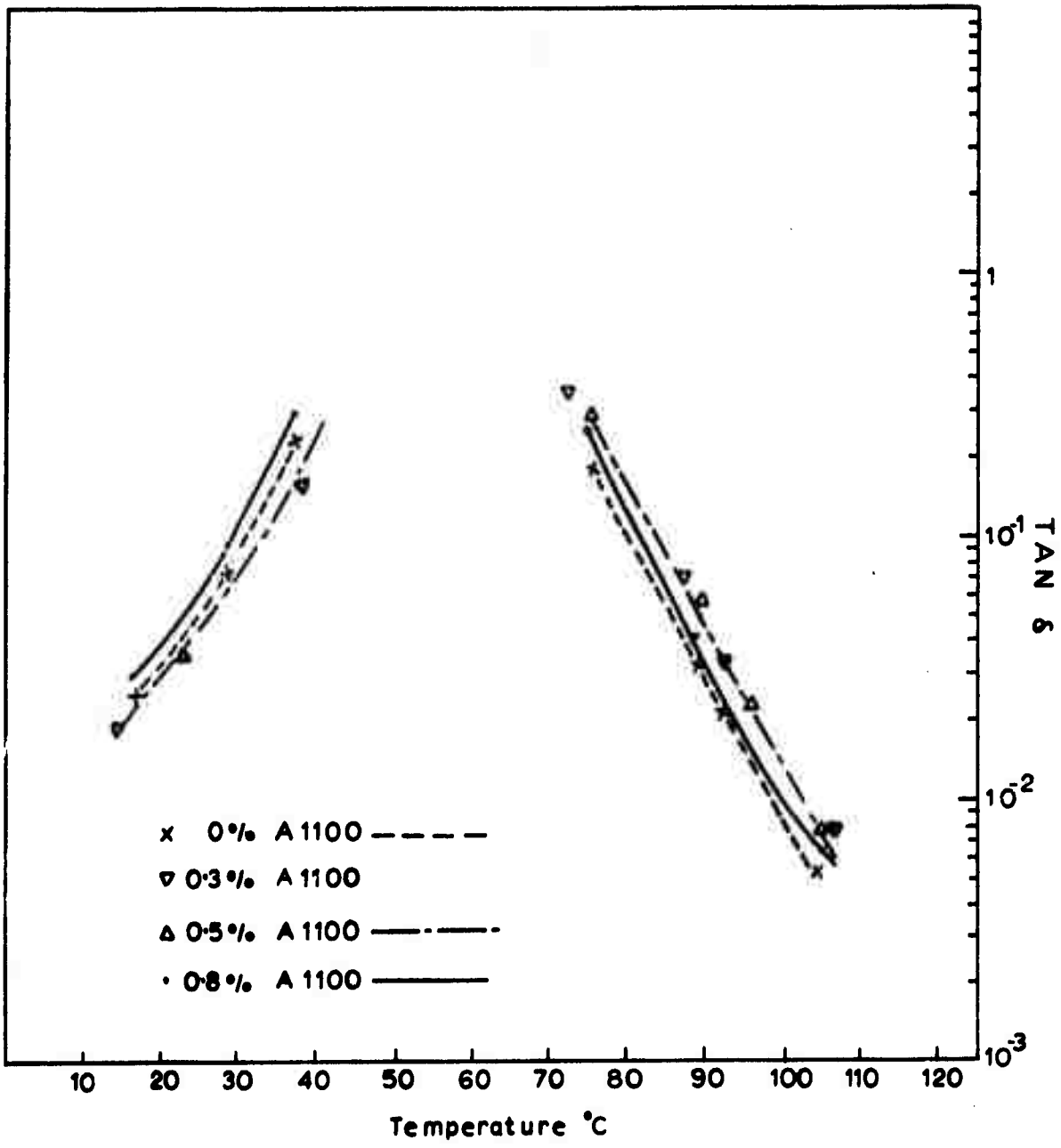

Fig 9. Effect of Amino-Silane Finish on Tan δ

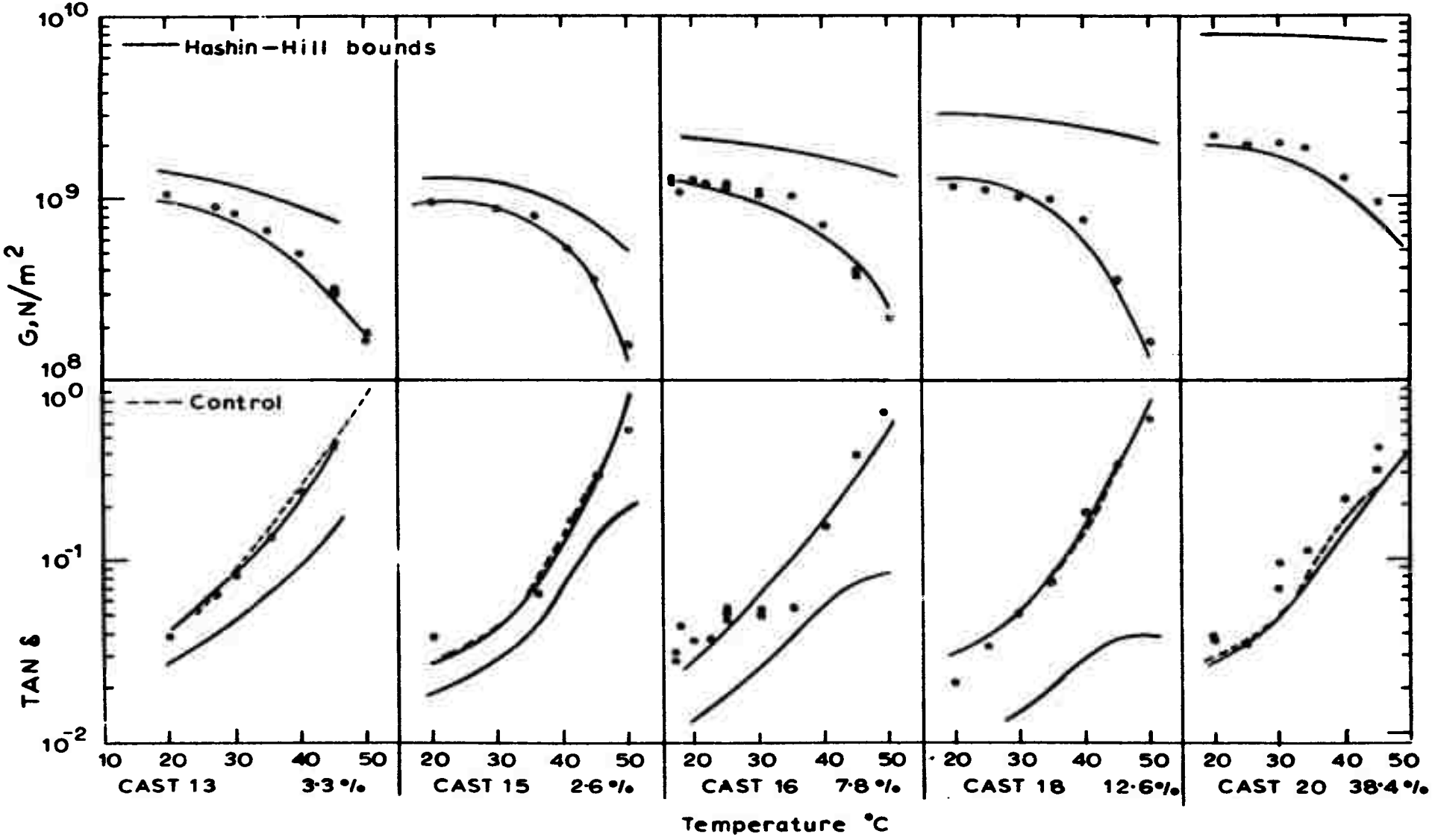

Fig 10. Results on Specimens cut with Axes at 0° to Fibres

Casts 13 to 20 Glassy State

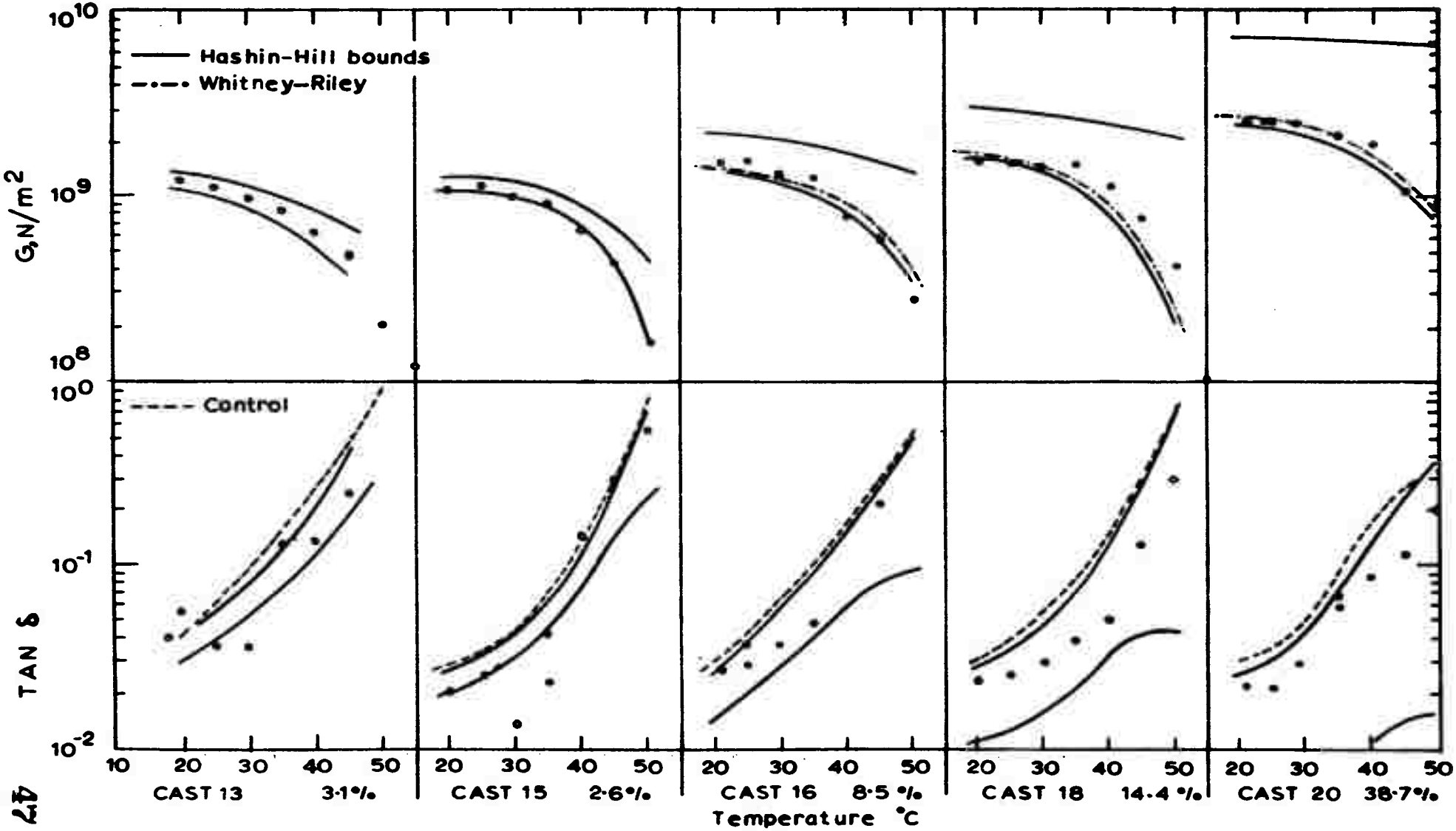

Fig 11. Results on Specimens Cut with Axes at 30° to Fibres

Casts 13 to 20 Glassy State

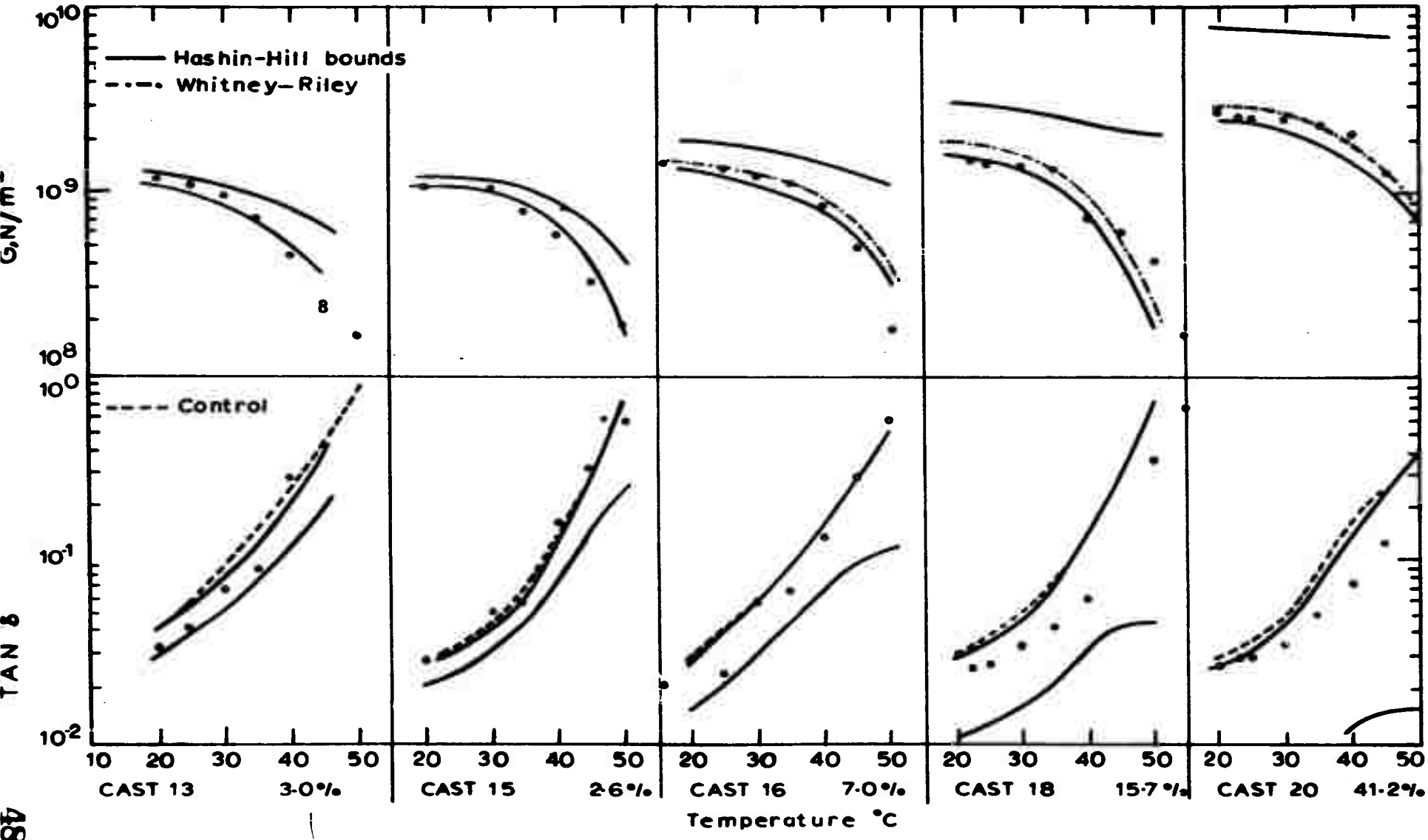

Fig 12. Results on Specimens Cut with Axes at 45° to Fibres

Casts 13 to 20 Glassy State

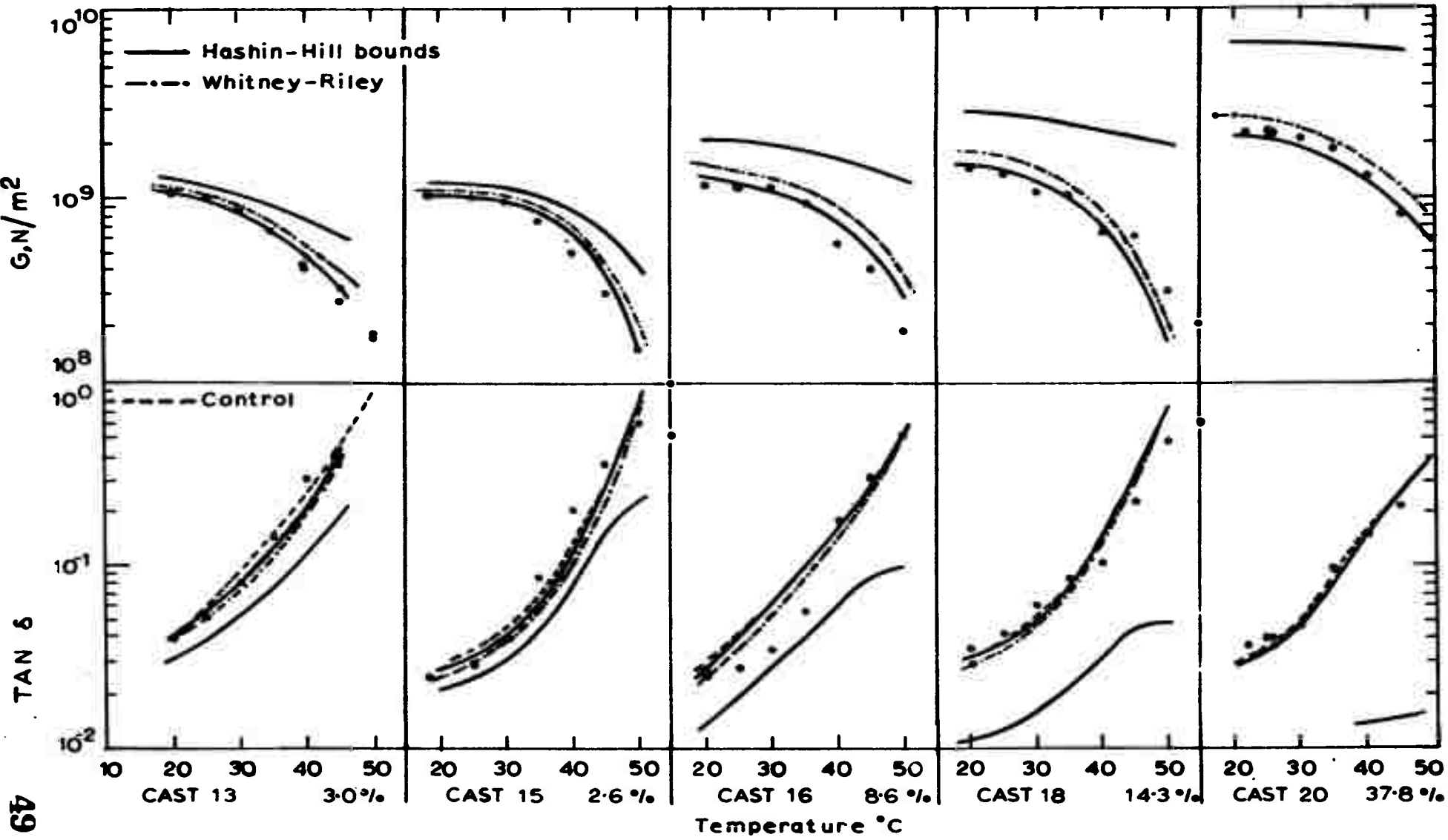

Fig 13. Results on Specimens Cut with Axes at 60° to Fibres

Casts 13 to 20 Glassy State

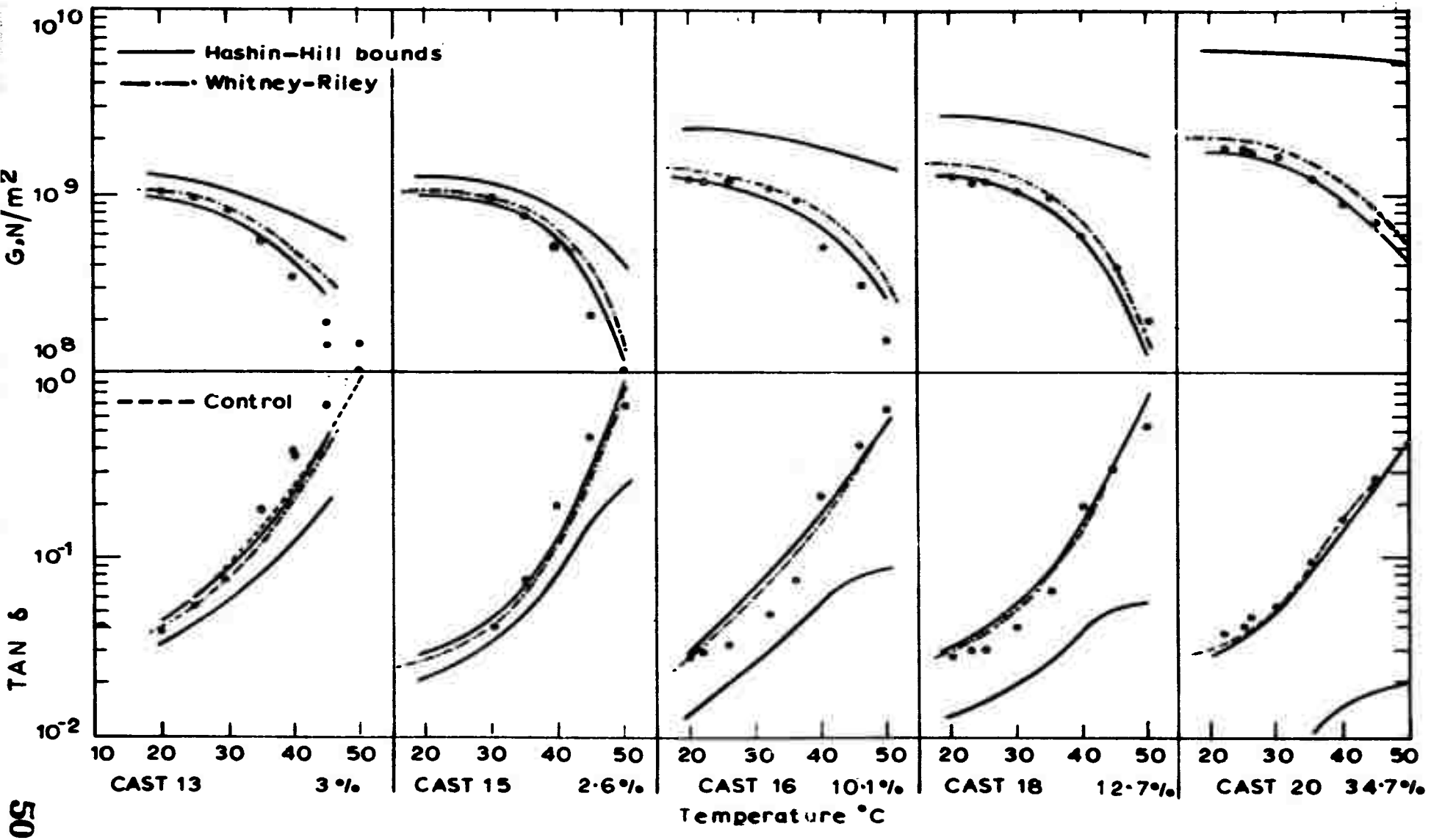

Fig 14. Results on Specimens Cut with Axes at 90° to the Fibres

Casts 13 to 20 Glassy State

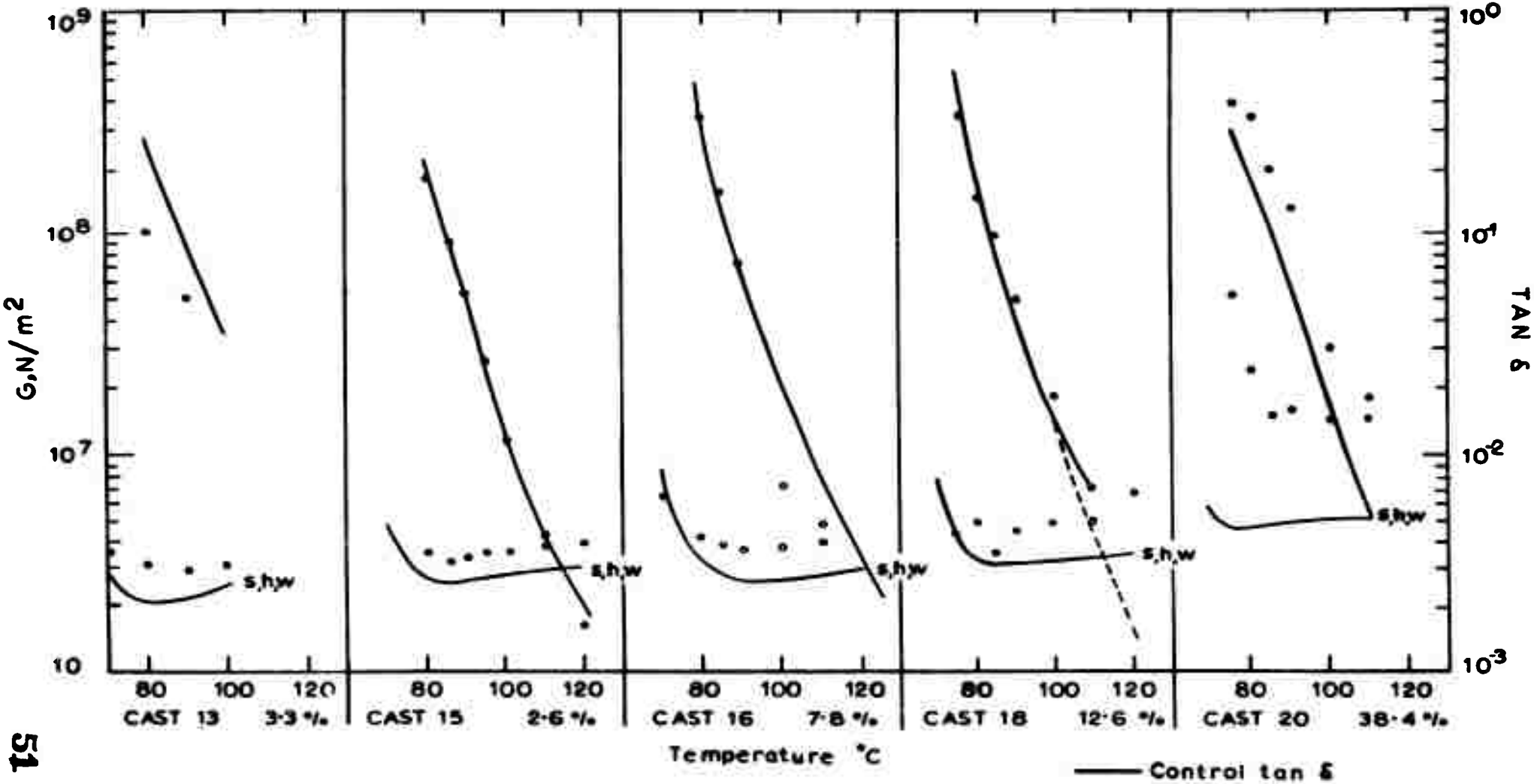

Fig 15. Results on Specimens Cut with Axes at 0° to the Fibres Compared with Theoretical Calculations and Control

Casts 13 to 20 Rubbery State

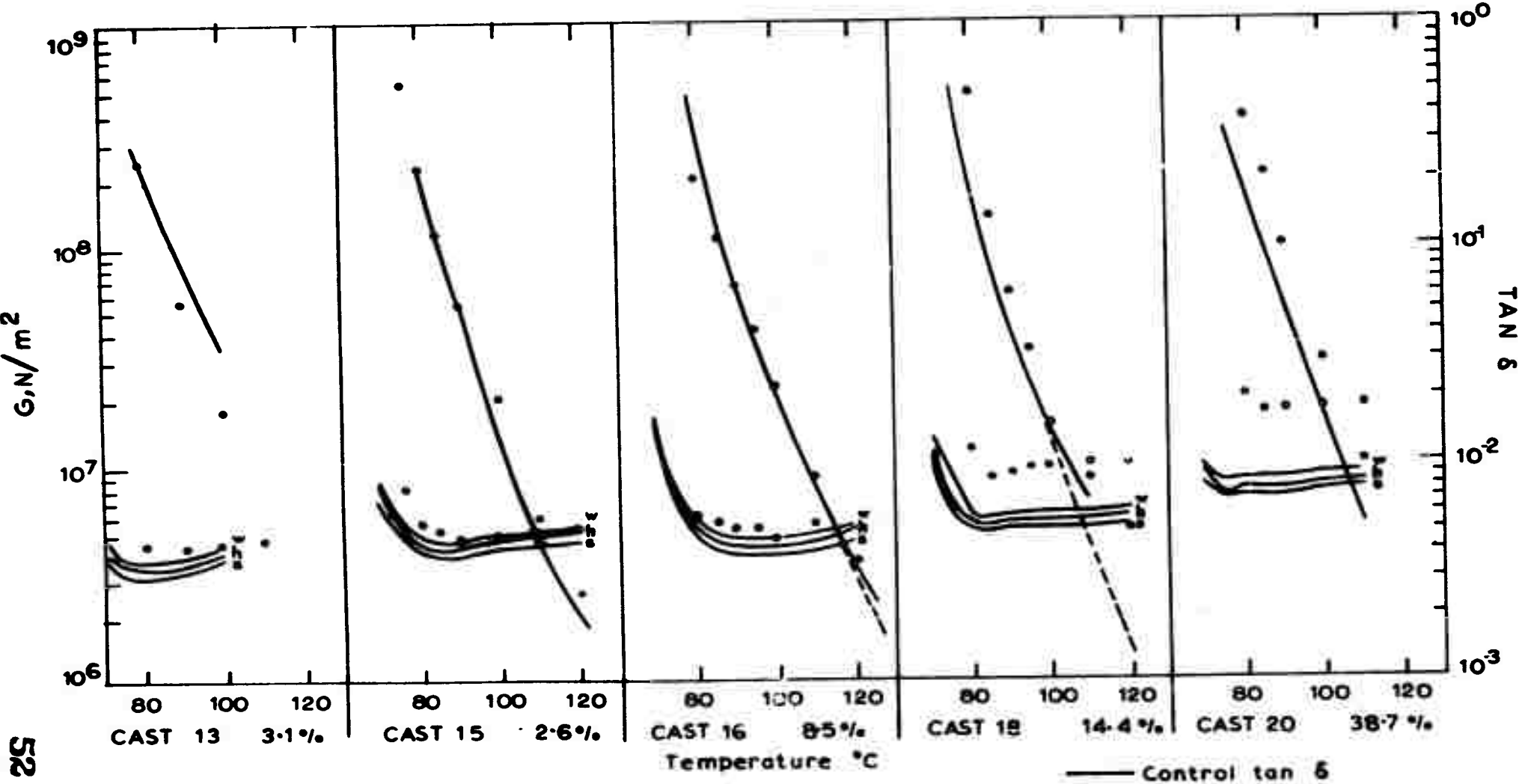

Fig 16. Results on Specimens Cut with Axes at 30° to the Fibres Compared with Theoretical Calculations and Control

Casts 13 to 20 Rubbery State

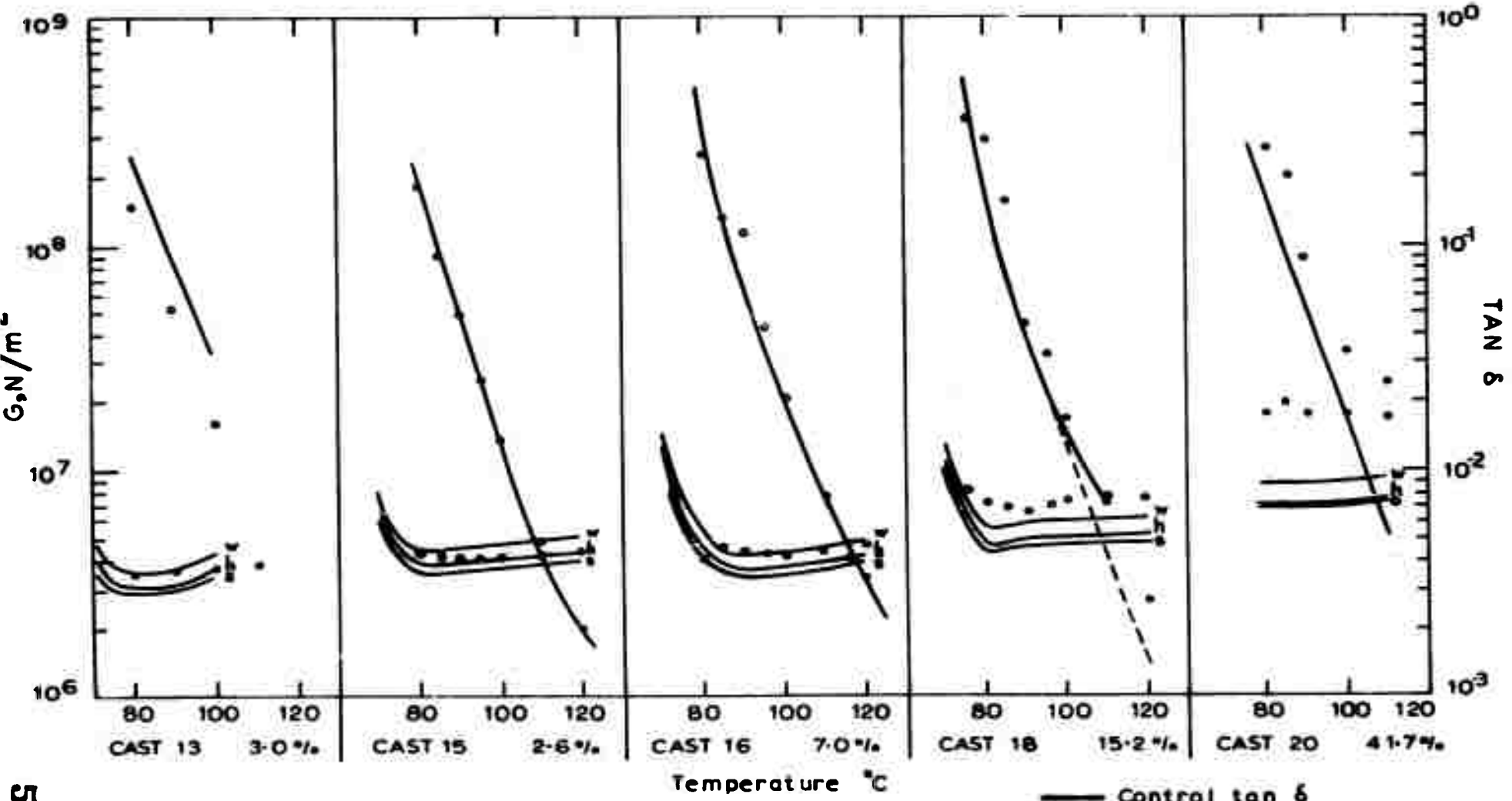

Fig 17. Results on Specimens Cut with Axes at 45° to Fibres Compared with Theoretical Calculations and Control

Casts 13 to 20 Rubbery State

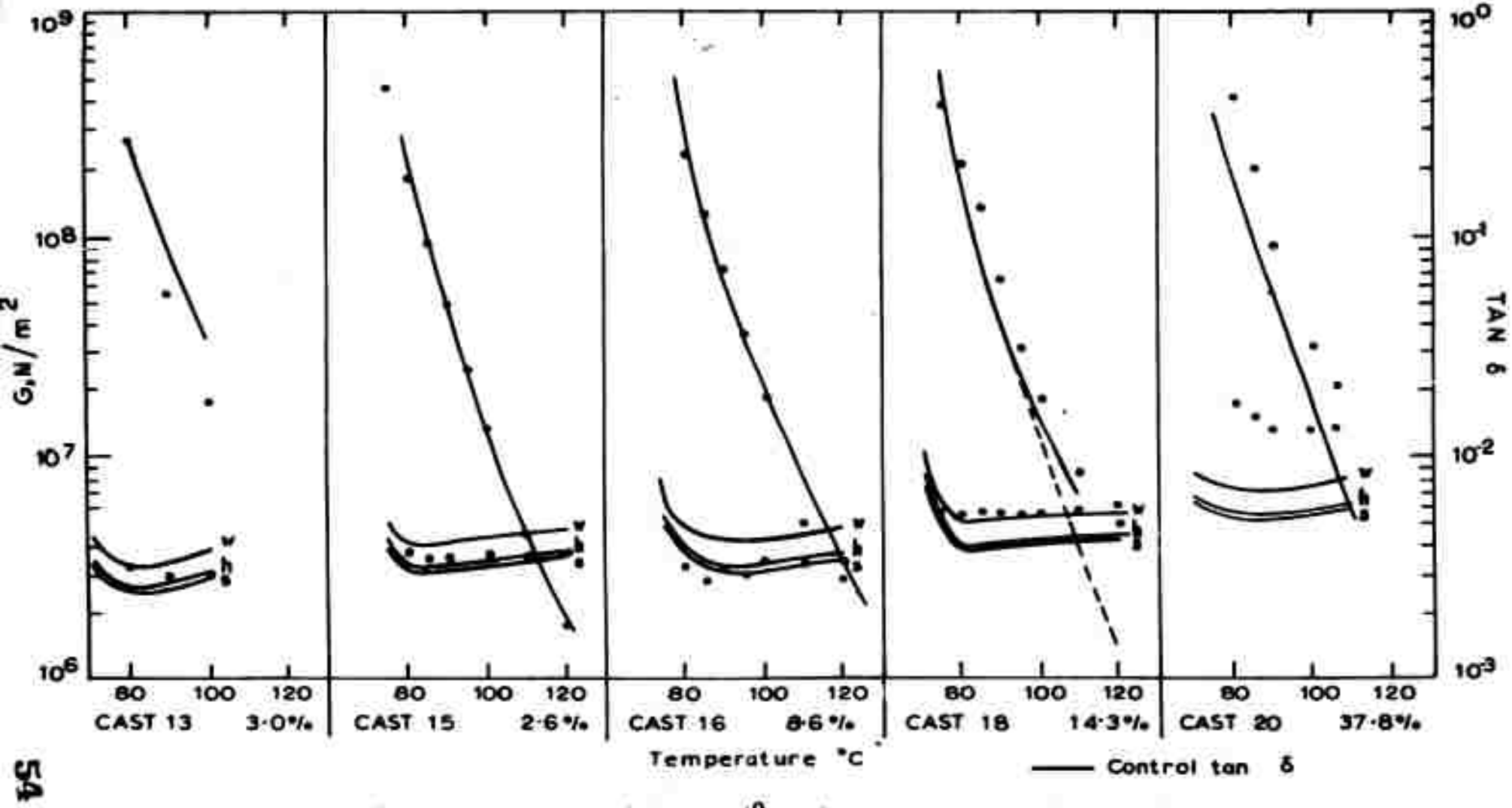

Fig 18. Results on Specimens Cut with Axes at 60° to Fibres Compared with Theoretical Calculations and Control

Casts 13 to 20 Rubbery State

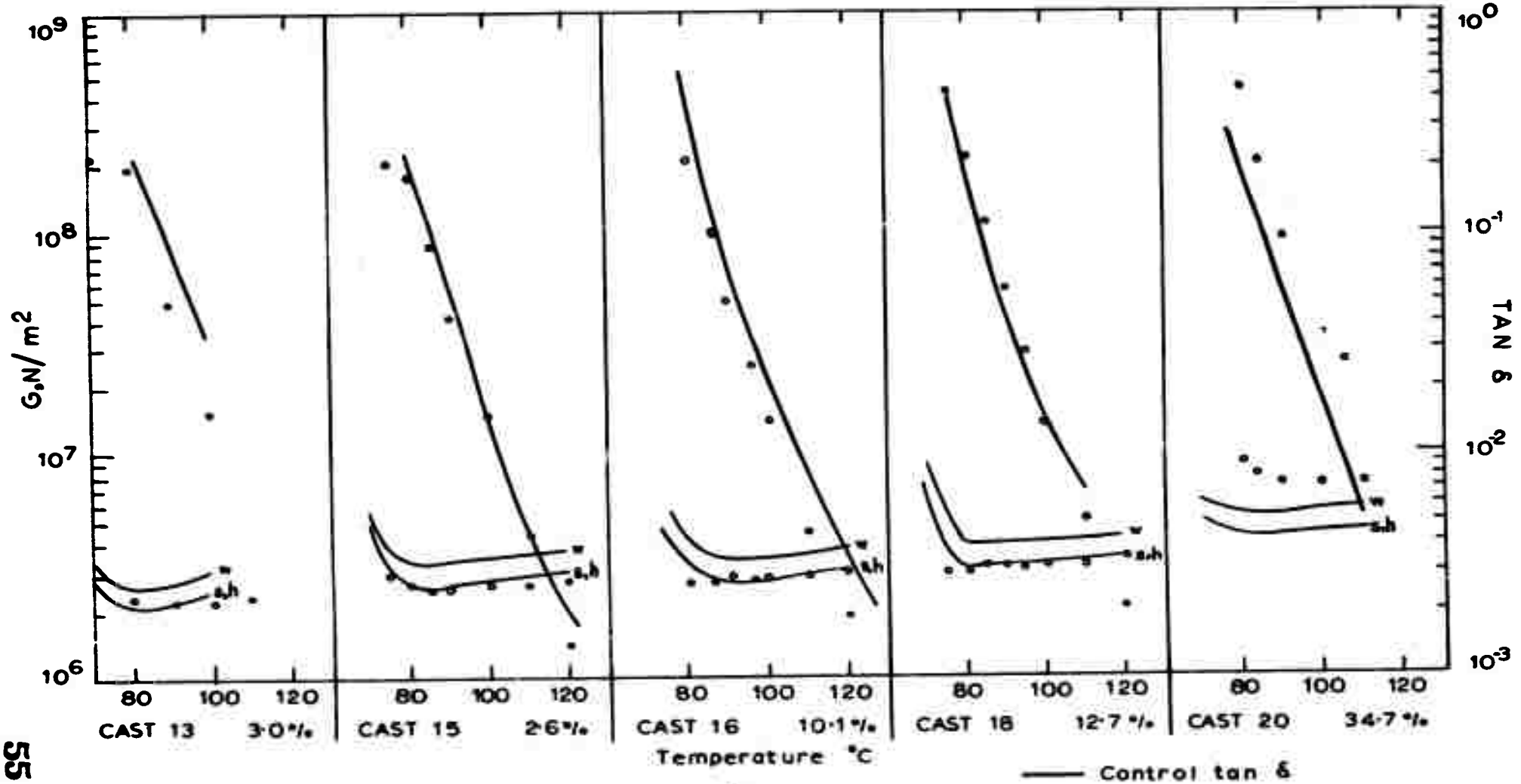

Fig 19. Results on Specimens Cut with Axes at 90° to Fibres Compared with Theoretical Calculations and Control

Casts 13 to 20 Rubbery State

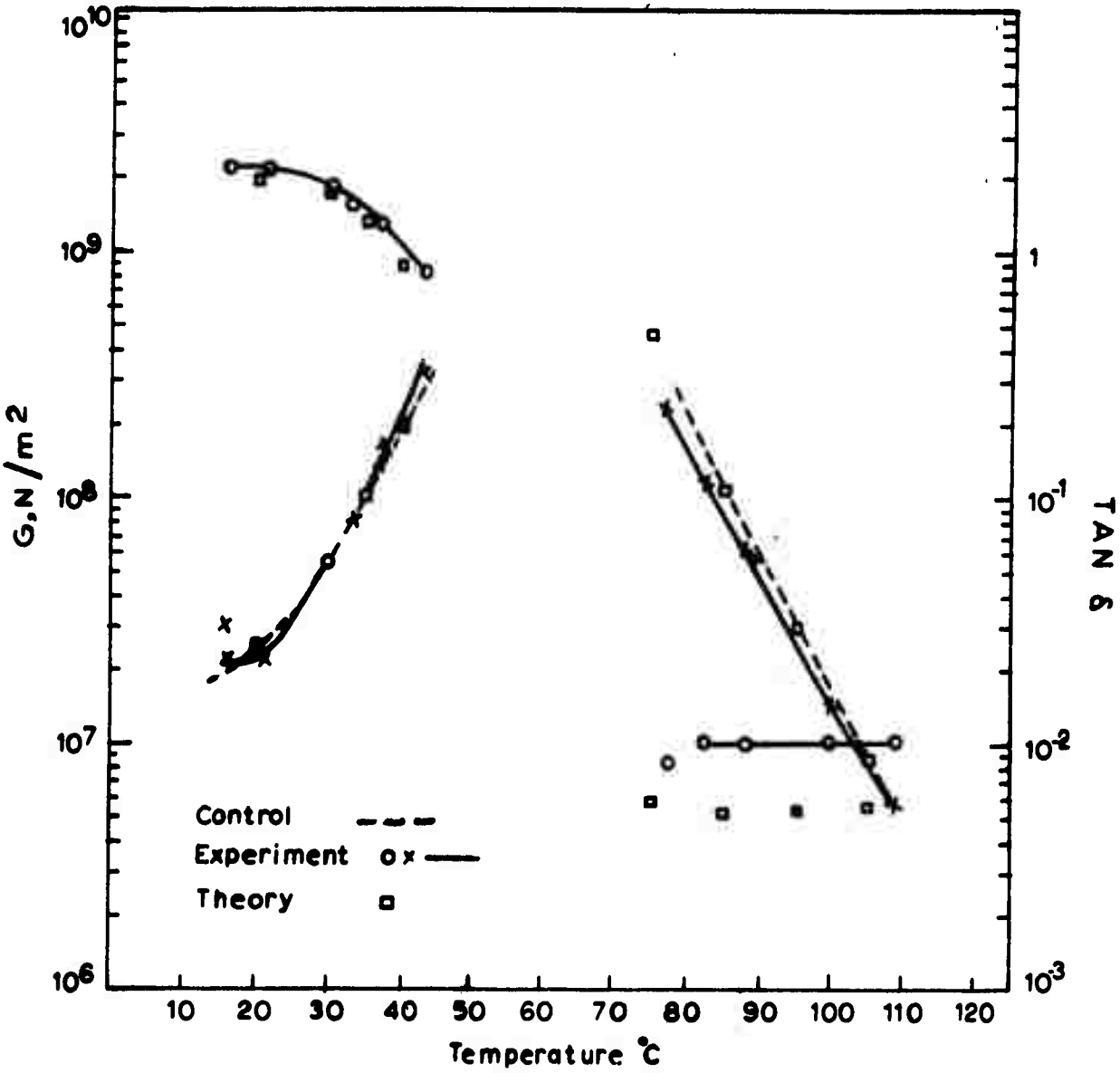

Fig 20. Comparison of results on specimens cut with Axes at 0° to Fibres with Theoretical Calculations and Control - No Finish on Glass Fibres

Cast 29, 33% Fibres

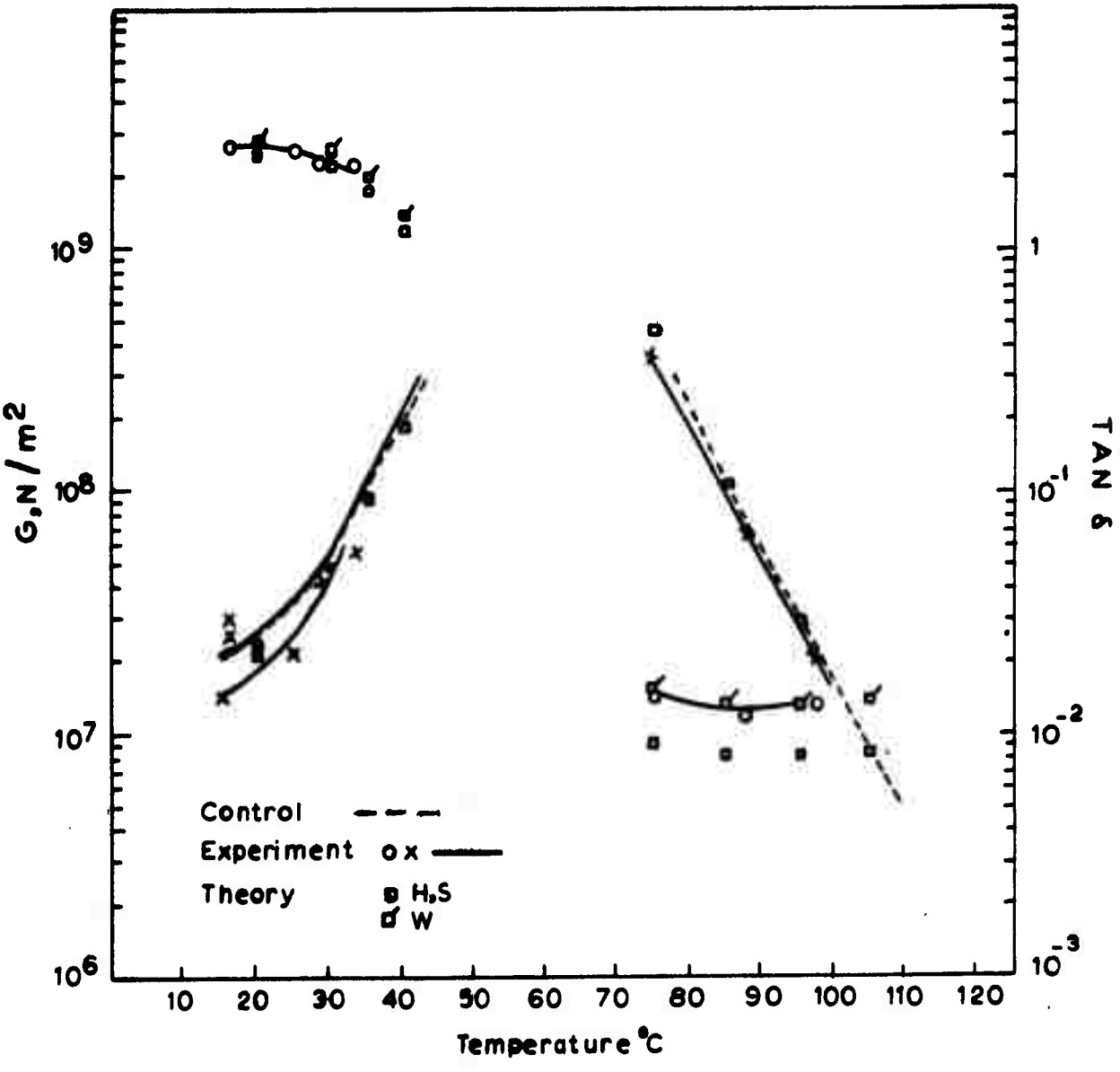

Fig 21 Comparison of results on Specimens cut with Axes at 30° to Fibres with Theoretical Calculations and Control - No Finish on Glass Fibres

Cast 29 31% Fibres

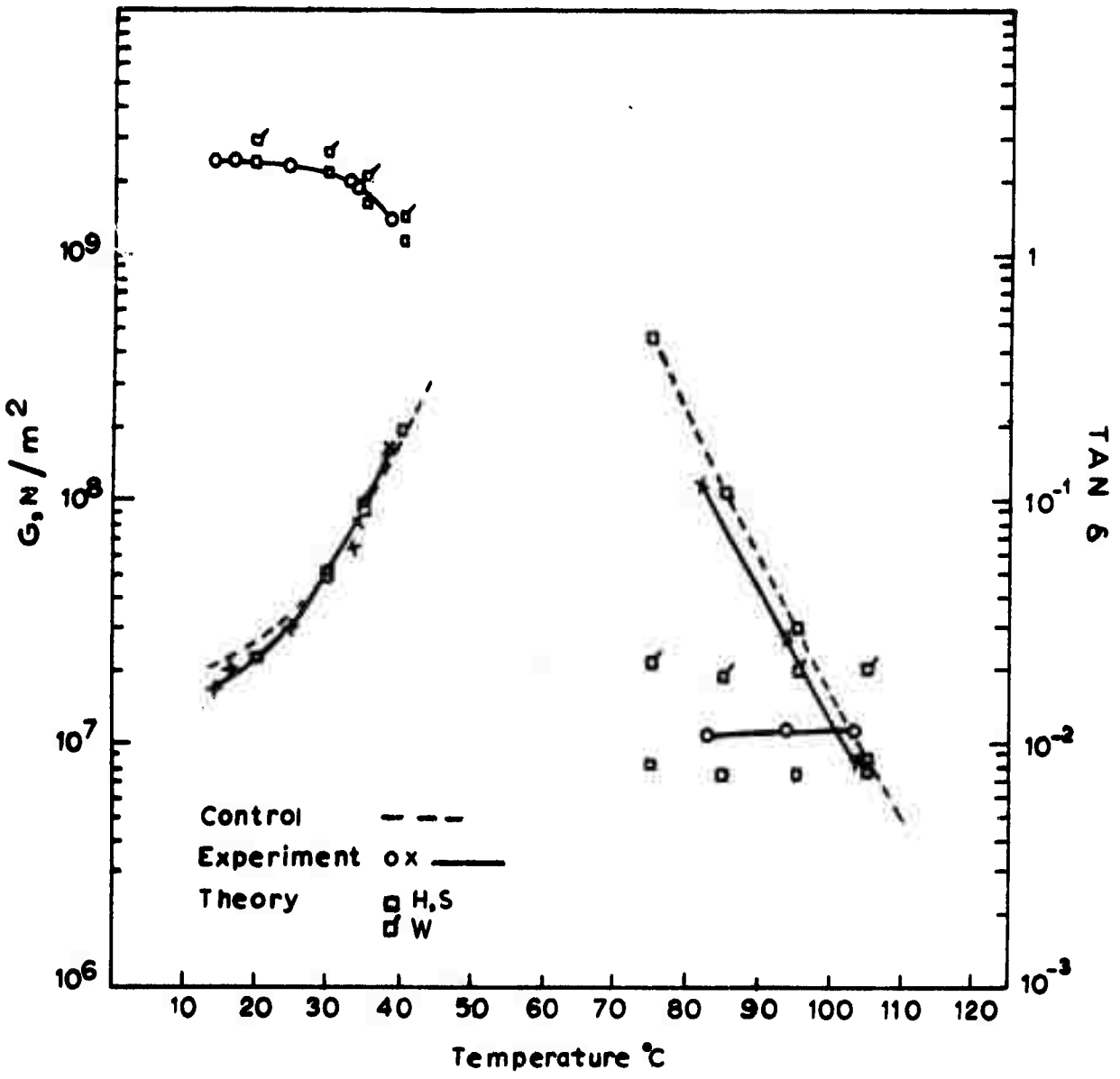

Fig 22 Comparison of results on Specimens cut with Axes at 45° to Fibres with Theoretical Calculations and Control - No Finish on Glass Fibres

Cast 29 32% Fibres

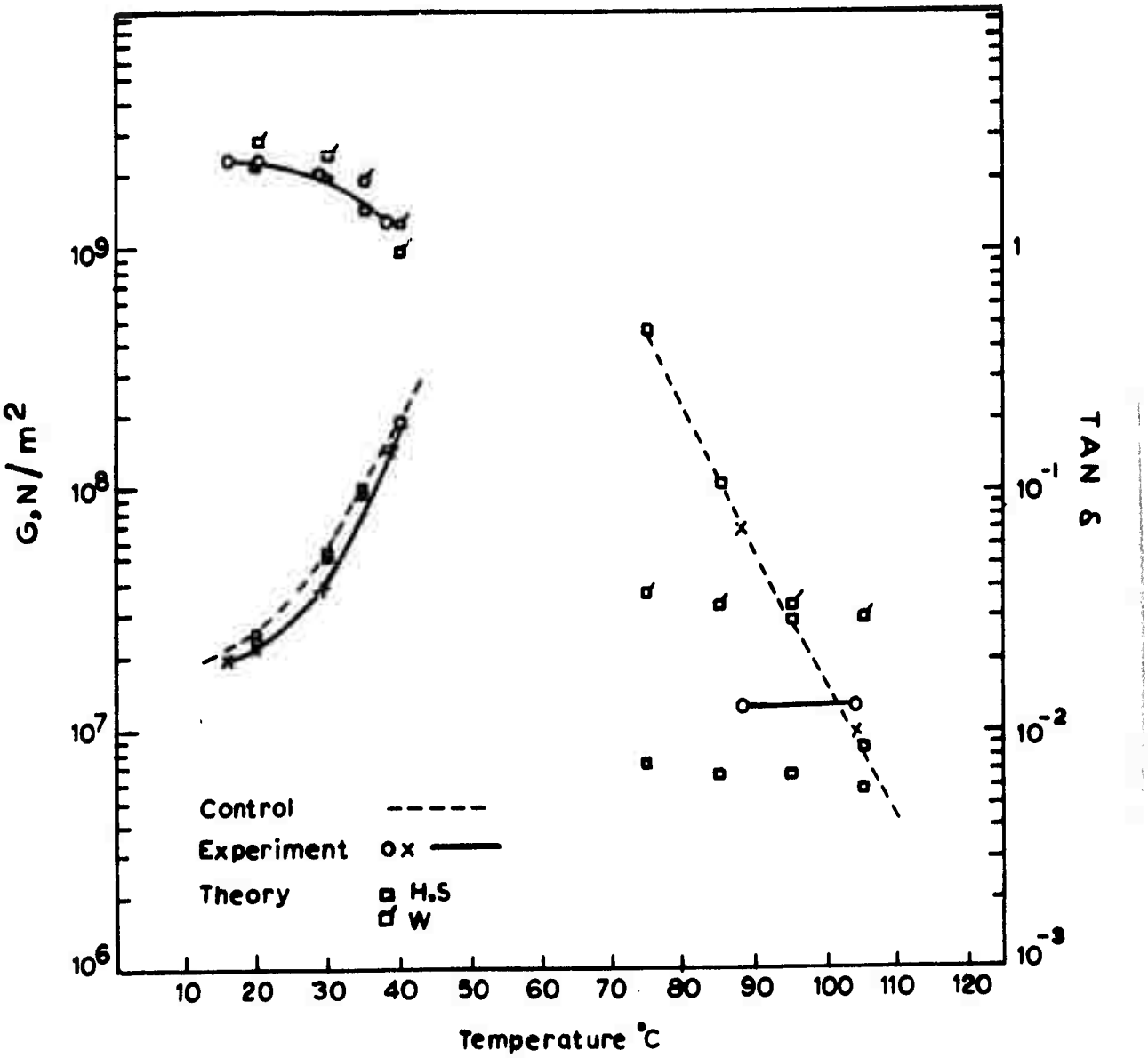

Fig 23 Comparison of results on Specimens cut with Axes at 60° to Fibres with Theoretical Calculations and Control - No Finish on Glass Fibres

Cast 29 31% Fibres

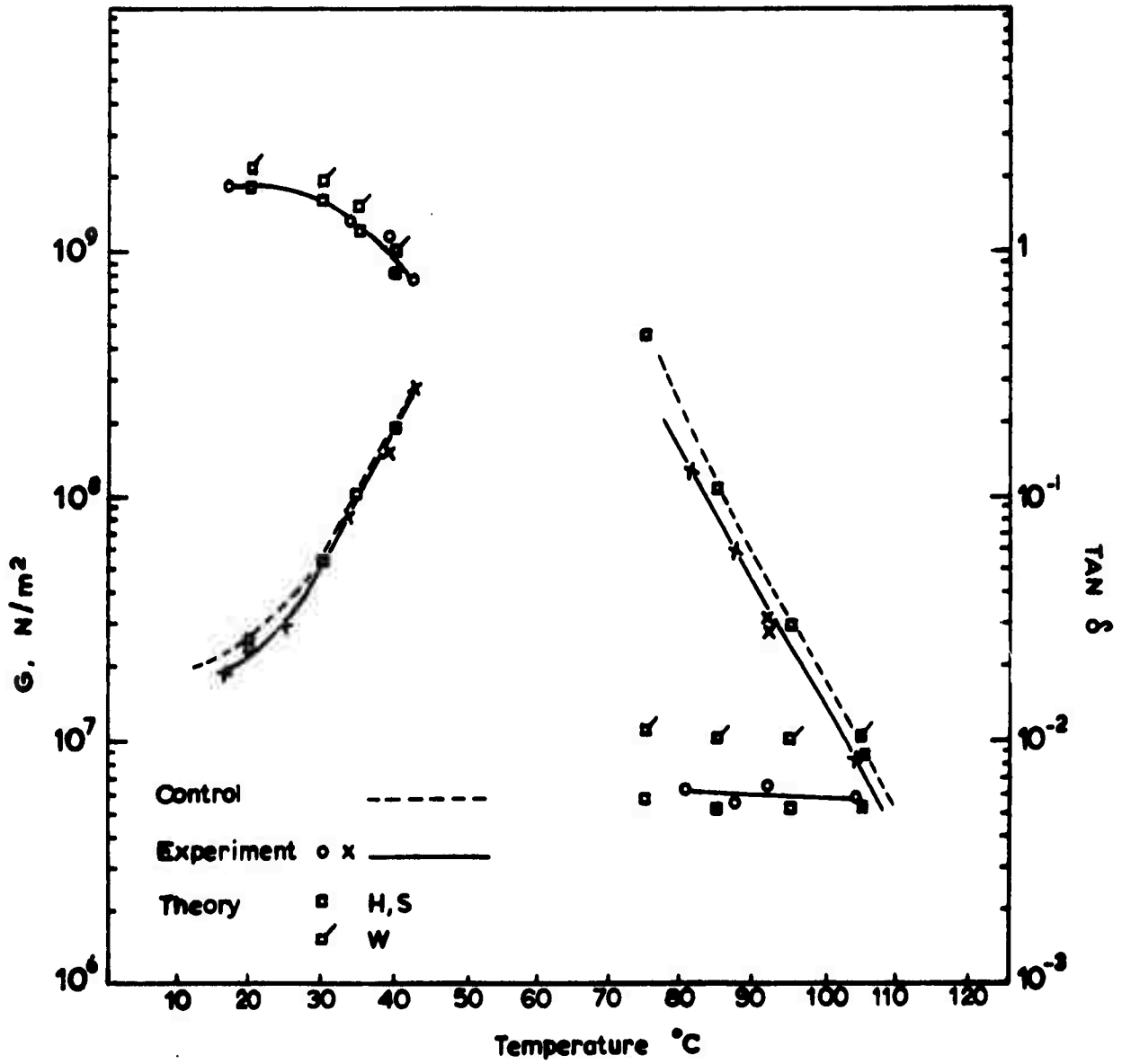

Fig 24. Comparison of results on Specimens cut with Axes at 90° to Fibres with Theoretical Calculations and Control - No Finish on Fibres

Cast 29 31% Fibres

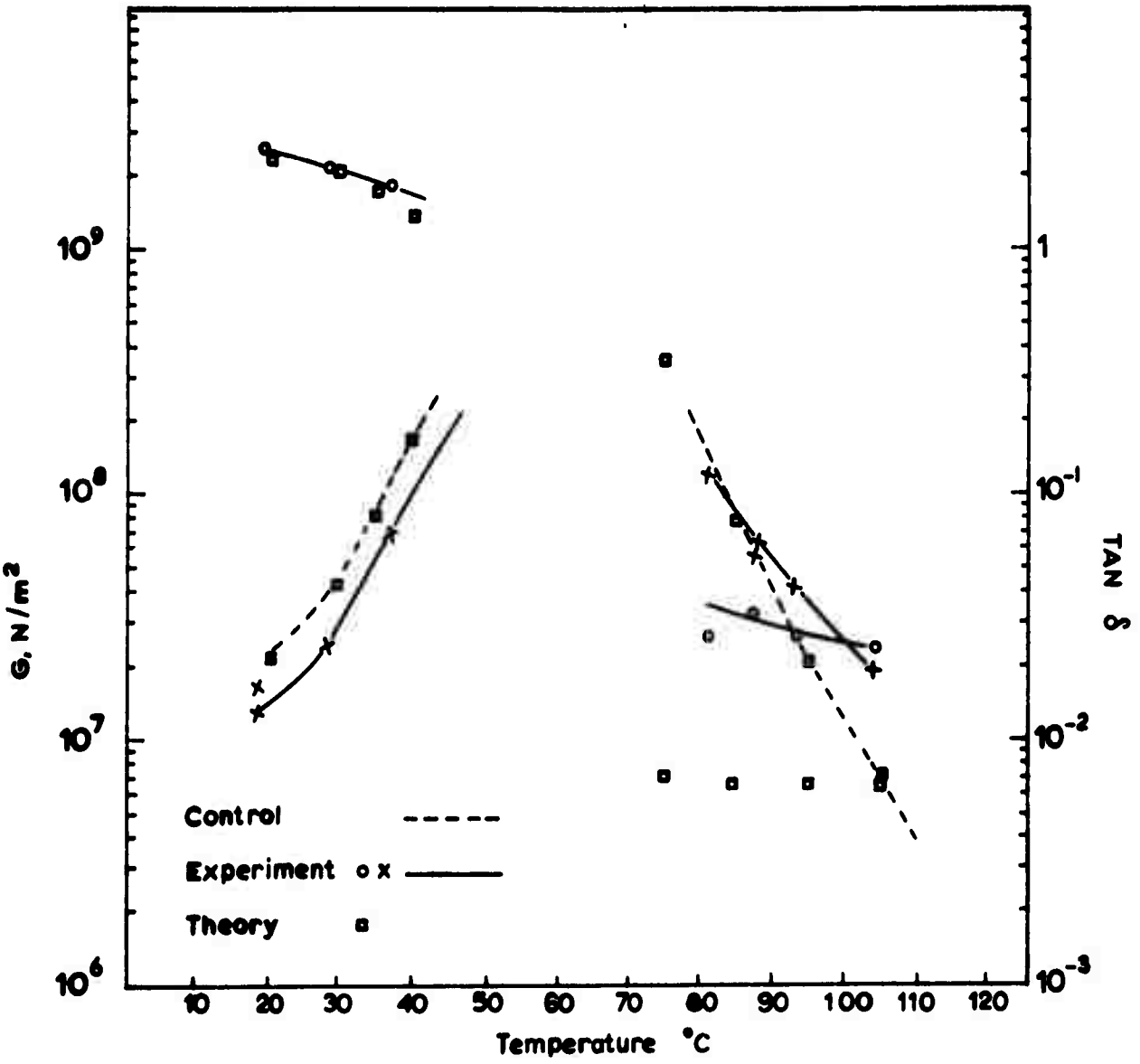

Fig 25. Comparison of results on Specimens cut with Axes at 0° to Fibres with Theoretical Calculations and Control-Finish on Fibres

Cast 30 41% Fibres

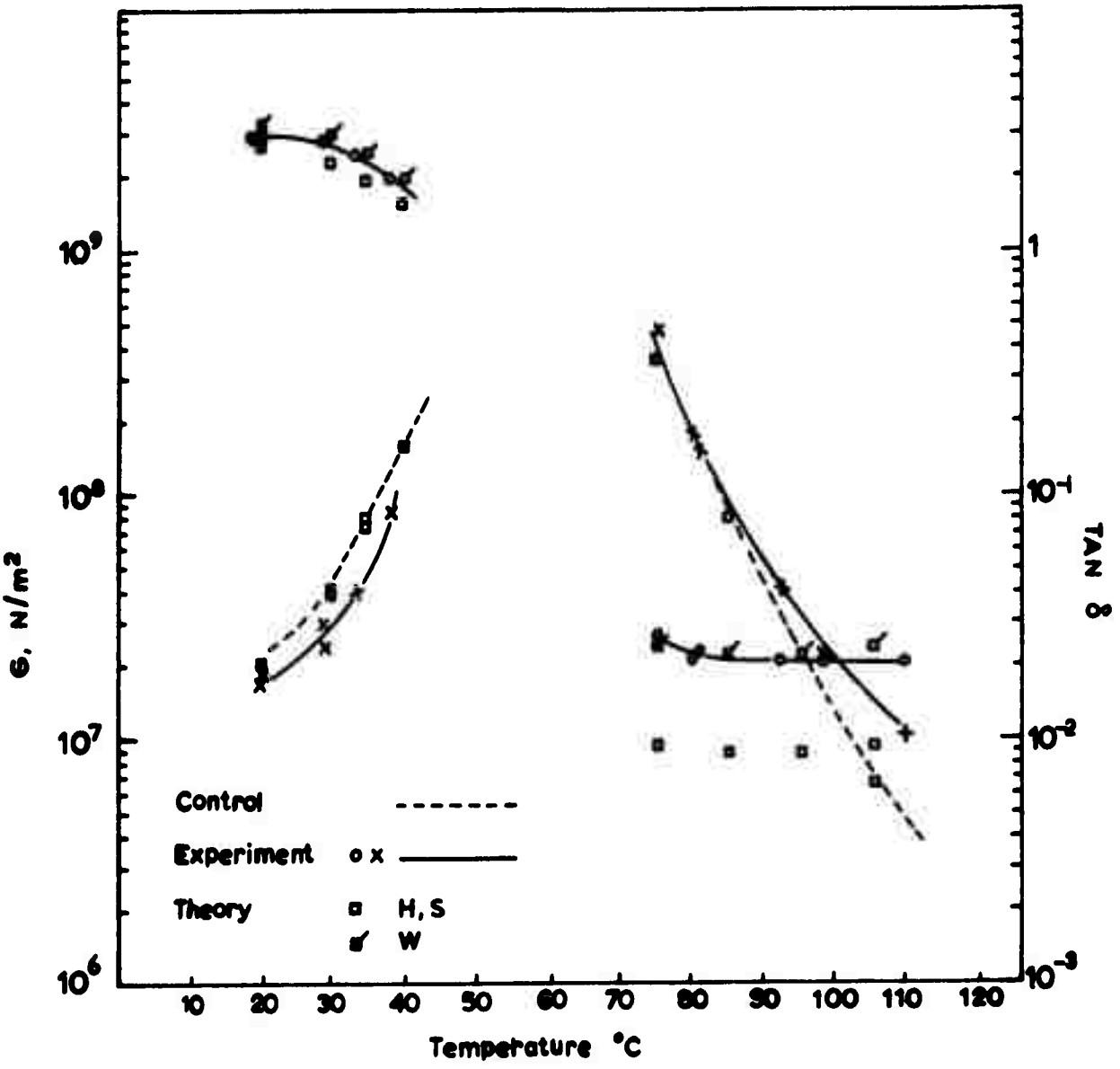

Fig 26. Comparison of results on Specimens cut with Axes at 45° to Fibres with Theoretical Calculations and Control-Finish on Fibres

Cast 30 37% Fibres

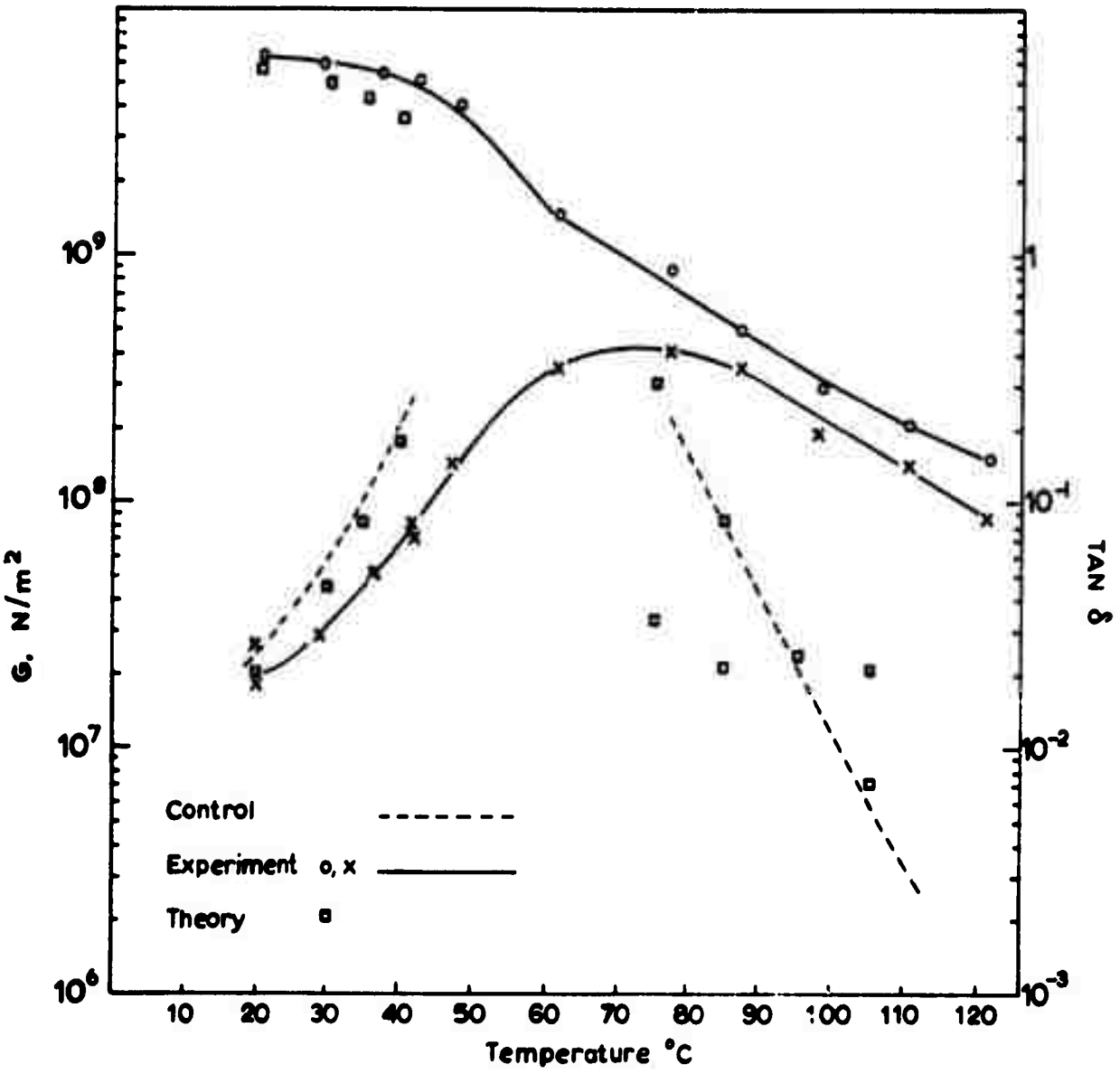

Fig 27. Comparison of results on Specimens cut with Axes at 0° to Fibres with Theoretical Calculations and Control - No Finish on Fibres

Cast 33 74% Fibres

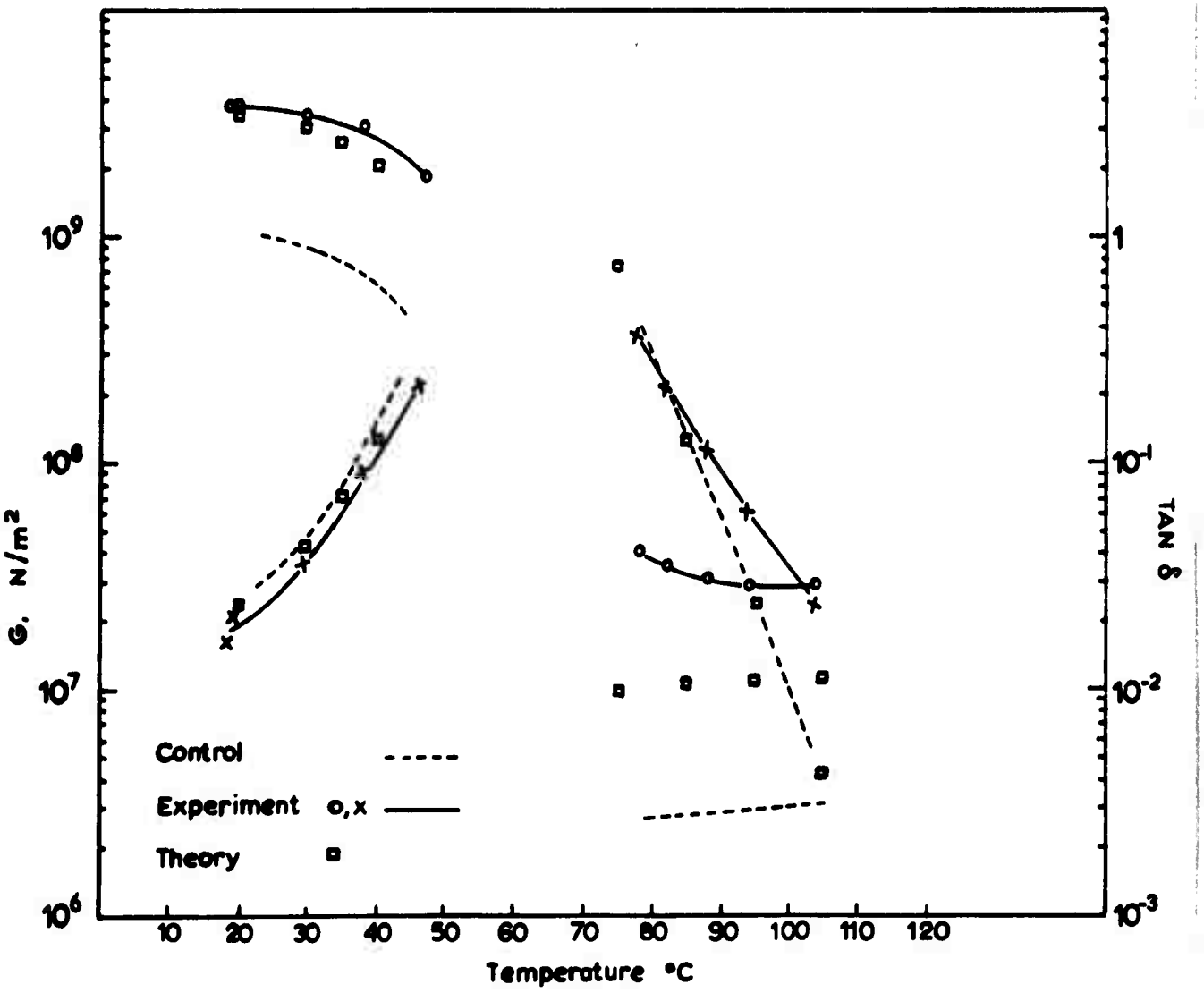

Fig 28. Comparison of results on Specimens cut with Axes at 0° to Fibres with Theoretical Calculations and Control - No Finish on Fibres

Cast 42 58% Fibres

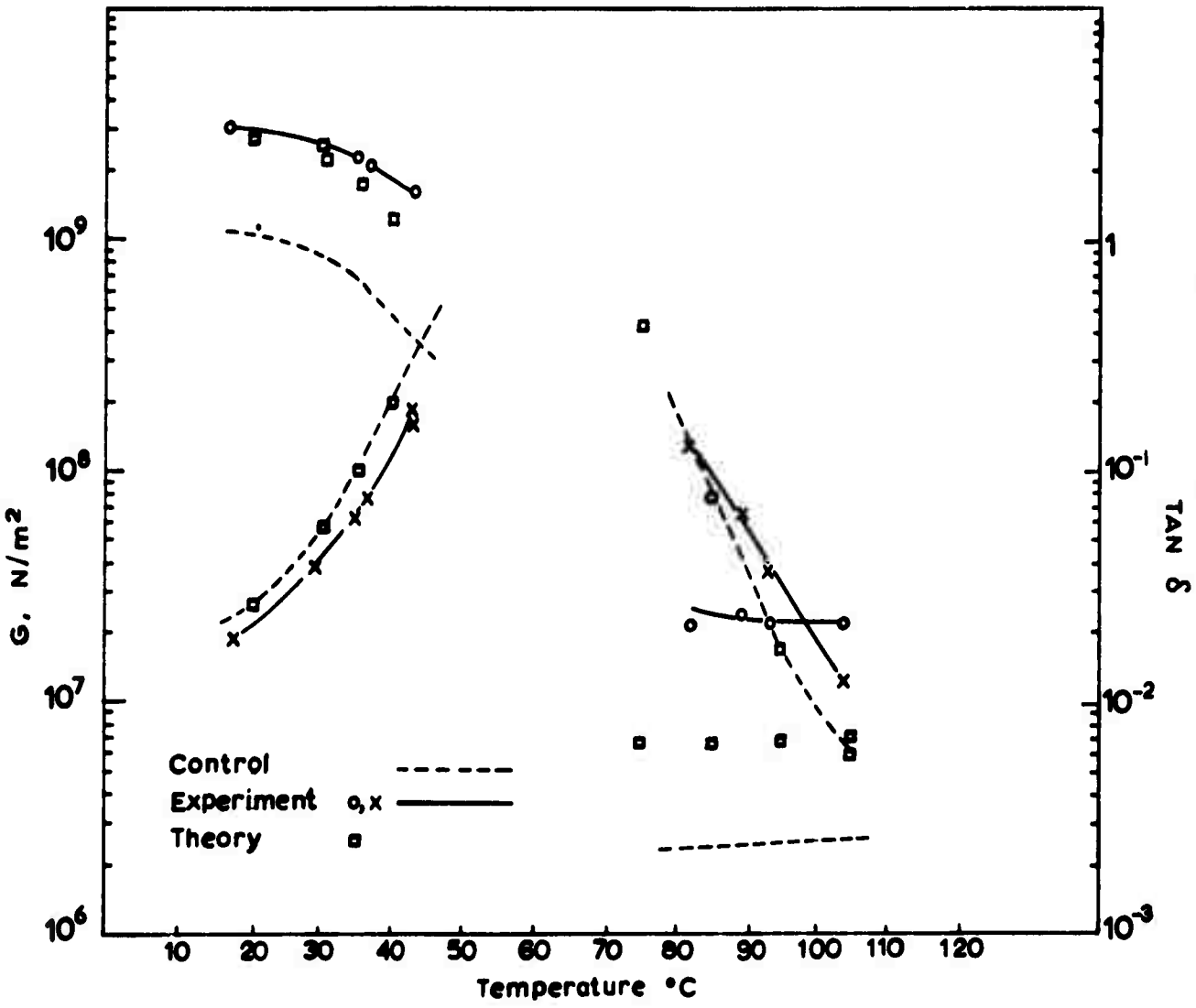

Fig 29. Comparison of results on Specimens cut with Axes at 0° to Fibres with Theoretical Calculations and Control - Finish on Fibres

Cast 34 48% Fibres

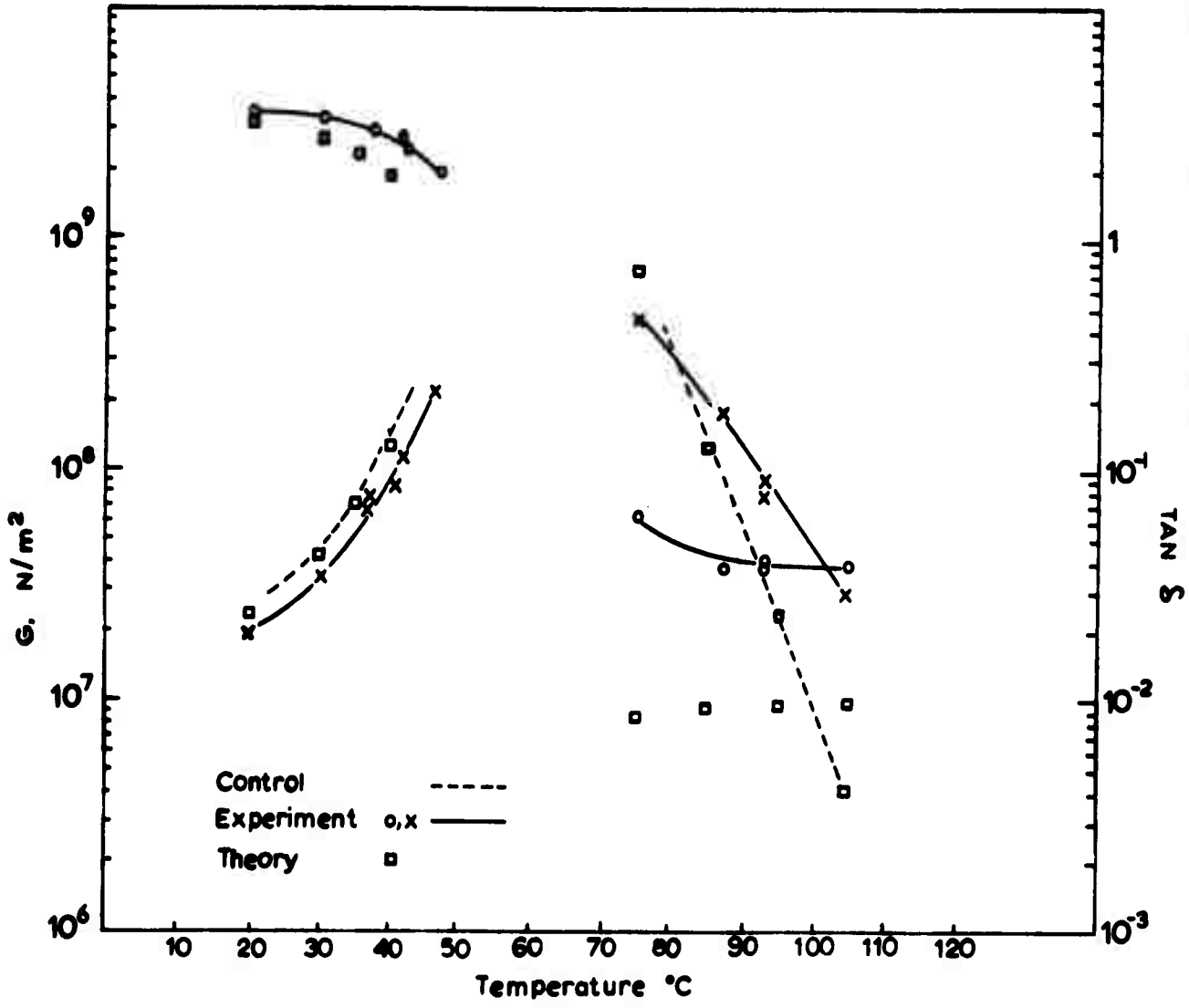

Fig 30. Comparison of results on Specimens cut with Axes at 0° to Fibres with Theoretical Calculations and Control - No Finish on Fibres

Cast 43 54% Fibres

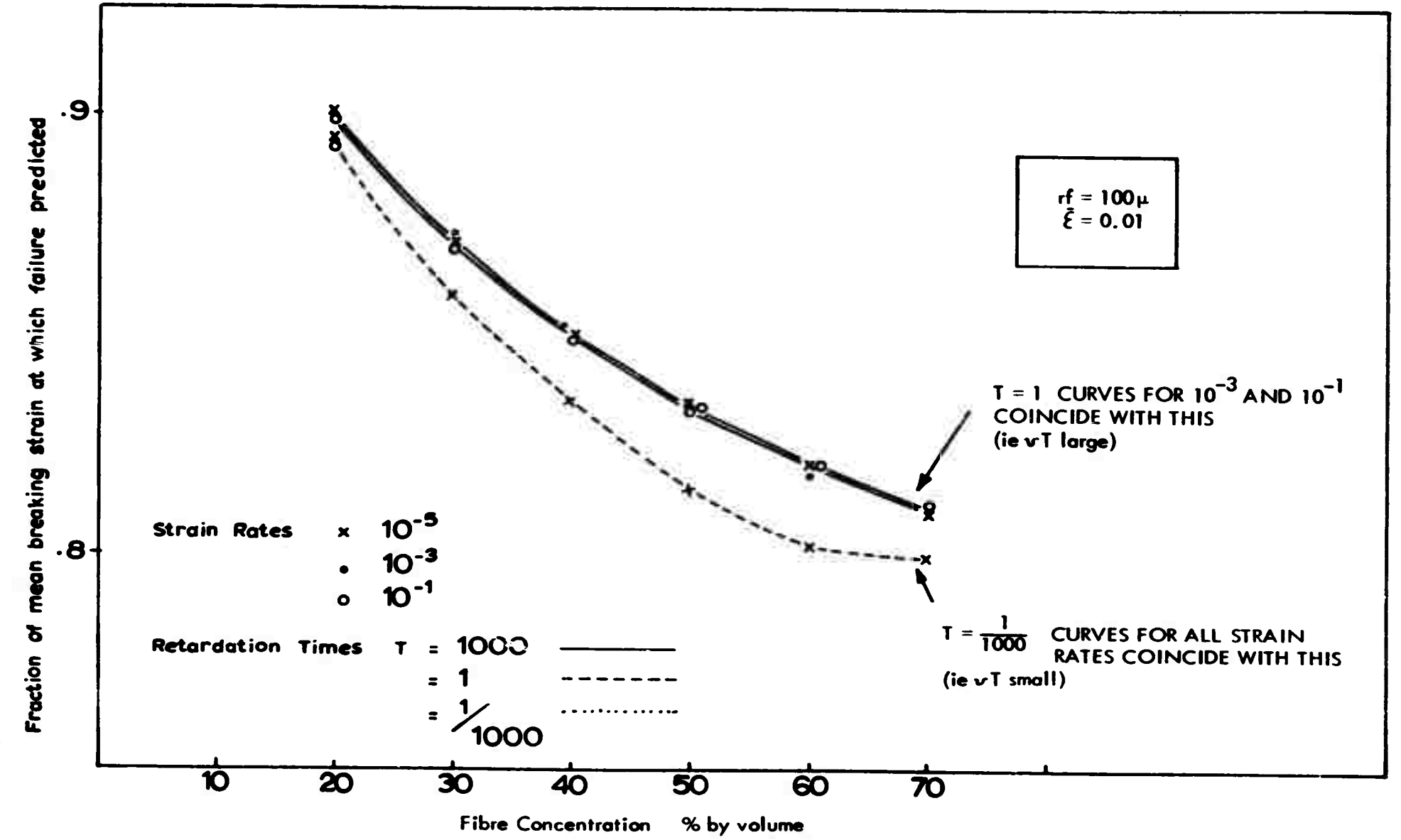

Fig 31. Graph of Predicted Failing Strain against Fibre Concentration for rf = 100μ, $\bar{\varepsilon}$ = 0.01

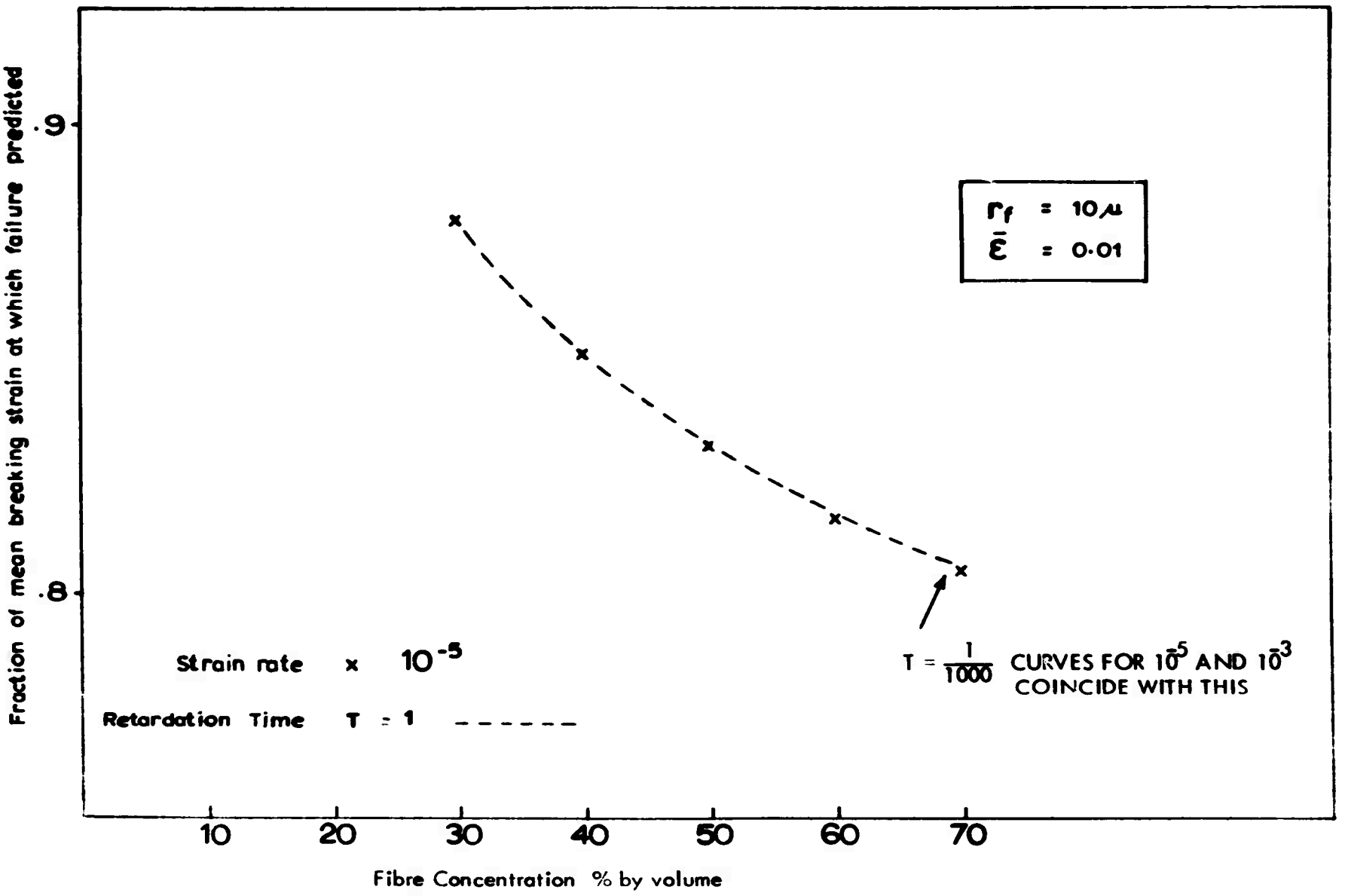

Fig 32. Graph of Predicted Failing Strain against Fibre Concentration for rf = 10μ, $\bar{\epsilon}$ = 0.01

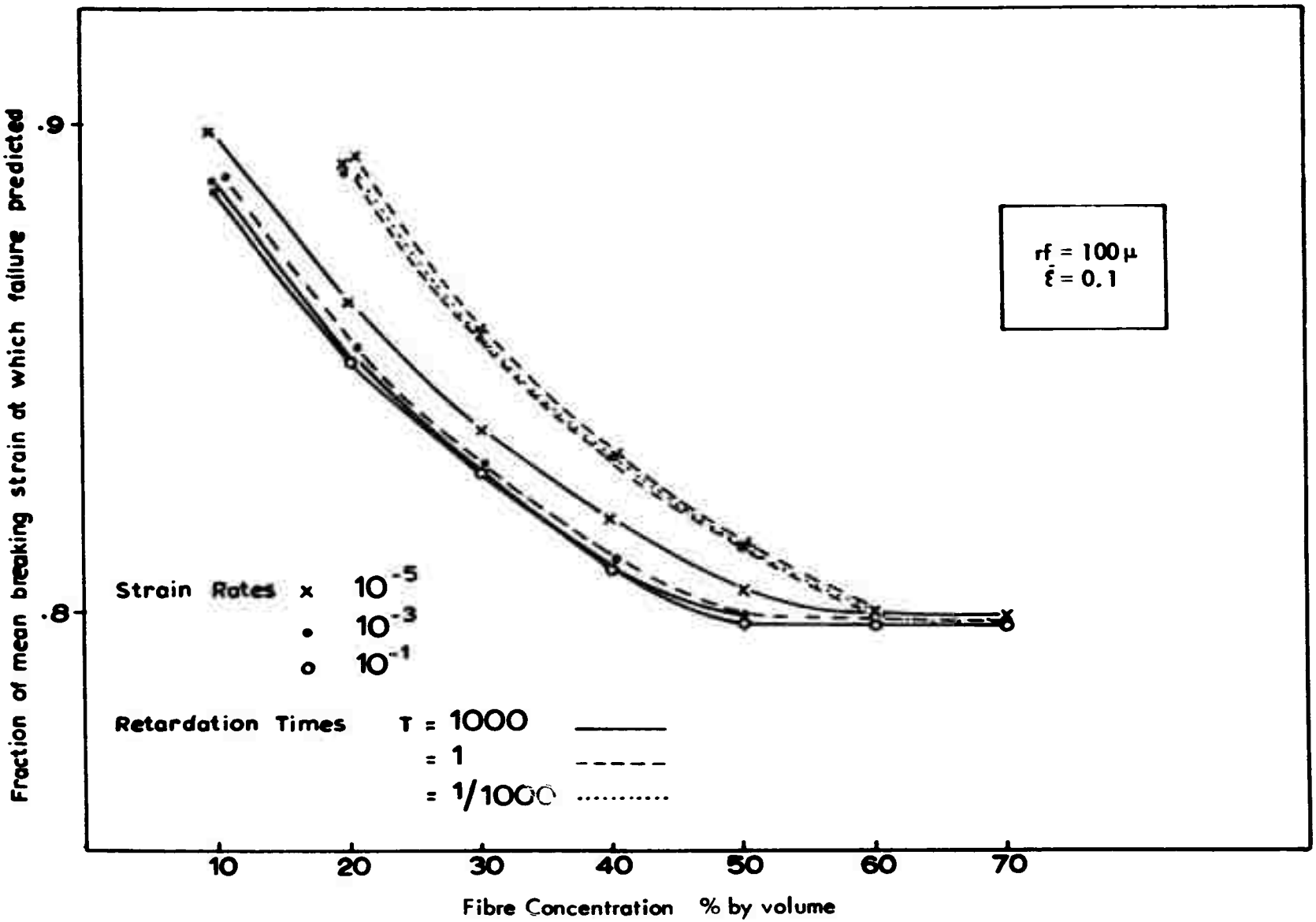

Fig 33. Graph of Predicted Failing Strain against Fibre Concentration for rf = 100 μ, $\bar{\varepsilon}$ = 0.1

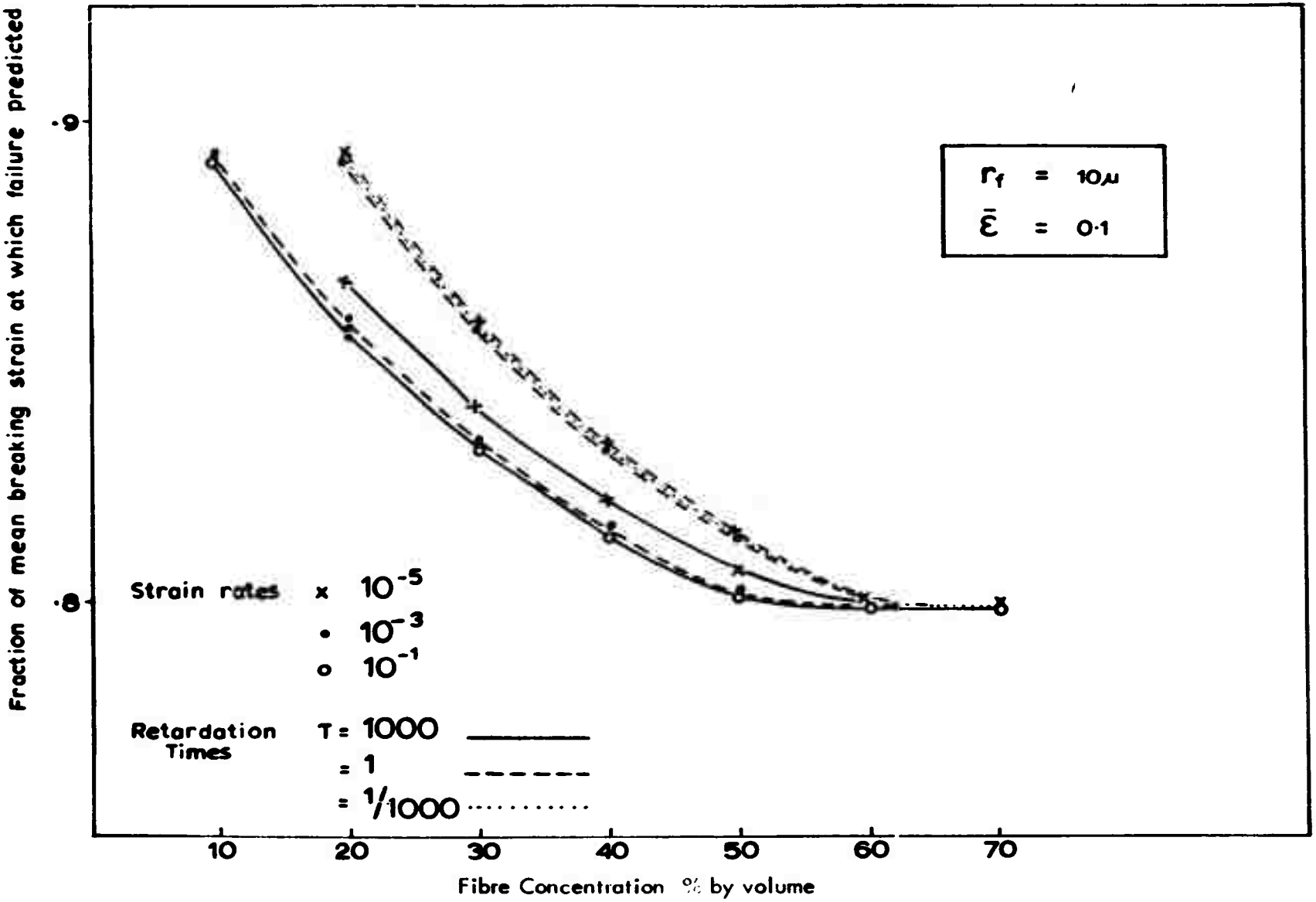

Fig 34. Graph of Predicted Failing Strain against Fibre concentration for rf = 10μ, $\bar{\varepsilon}$ = 0.1